Chapter 17

Random Fatigue Under Uniaxial and Multiaxial Loading Conditions

Chapter details

Chapter DOI:

https://doi.org/10.4322/978-65-86503-88-3.c17

Chapter suggested citation / reference style:

Ferreira, Jorge L. A., et al. (2022). “Random Fatigue Under Uniaxial and Multiaxial Loading Conditions”. *In* Jorge, Ariosto B., et al. (Eds.) *Uncertainty Modeling: Fundamental Concepts and Models*, Vol. III, UnB, Brasilia, DF, Brazil, pp. 552–612. Book series in Discrete Models, Inverse Methods, & Uncertainty Modeling in Structural Integrity.

P.S.: DOI may be included at the end of citation, for completeness.

Book details

Book: Uncertainty Modeling: Fundamental Concepts and Models

Edited by: Jorge, Ariosto B., Anflor, Carla T. M., Gomes, Guilherme F., & Carneiro, Sergio H. S.

Volume III of Book Series in:

Discrete Models, Inverse Methods, & Uncertainty Modeling in Structural Integrity

Published by: UnB City: Brasilia, DF, Brazil Year: 2022

DOI: https://doi.org/10.4322/978-65-86503-88-3

Random Fatigue Under Uniaxial and Multiaxial Loading Conditions

Jorge Luiz de A. Ferreira[1*], Felipe M. de Lima[2] and Emanuely U. Cardoso[3]

[1] Post-Graduate Program - Integrity of Engineering Materials, University of Brasilia, Brazil. Email:jorge@unb.br
[2] Post-Graduate Program - Mechanical Sciences (Fatigue, Fracture and Materials Group, GFFM/PCMEC), University of Brasilia, Brazil. E-mail:felipe.maganhalima@gmail.com
[3] Post-Graduate Program - Integrity of Engineering Materials, University of Brasilia, Brazil, E-mail:emanuely.ugulino@gmail.com

Abstract

Fatigue life prediction under multiaxial loading has become a fundamental part of product development for industries in areas such as aeronautics, offshore, automotive, and power generation, among others. Among the reasons can be mentioned the need to increase the safety and performance levels of structural components, together with the popularization of the use of computational tools capable of allowing the modeling of complex component geometries under any type of load. Although the computational packages used in these analyzes have several fatigue models, research is still needed to improve their life prediction capacity and computational efficiency, especially in the presence of random multiaxial loads. This is mainly because fatigue analysis under multiaxial random loading is still a task that is erroneously considered to be extremely complex. In this sense, this monograph is dedicated to presenting a comprehensive review of the concepts needed to understand the multiaxial random fatigue criteria available in the literature. Such a review is mainly devoted to stress-based criteria for the evaluation of fatigue life in high-cycle regime using the Maximum Variance Method. Time and frequency domain approaches are examined. To level the knowledge necessary to use the methodologies, a detailed review of the literature is presented on i) stochastic processes and characterization of loading histories (sections 1 and 2), ii) Material Fatigue and Uniaxial Random Fatigue Analysis (sections 3 to 5), iii) Fatigue multiaxial and Maximum Variance Methods using the Critical Plane approach (sections 6 to 8) iv) Fatigue multiaxial and Projection-by-Projection criteria (PbP) (section 9)

Keywords: life prediction; multiaxial loading; multiaxial random fatigue criteria; stochastic processes; characterization of loading histories; maximum variance method; Projections-by-Projection critical planes.

1 Introduction

Many mechanical and civil structures are subject to loads that vary essentially randomly throughout their lifetime. These loadings are, in general, caused by the most diverse sources (such as:

sea waves, winds, earthquakes, vehicle traffic, etc.). Fig. 1 are exemplified some of the possible loading histories observed in real situations.

These loading histories can be induce a mode of structural failure known as fatigue. Roughly speaking, fatigue can be defined as a process of localized damage and the cumulative one consisting of the beginning of the crack, the propagation, and the final fracture of a component. Typically, the final fracture occurs without notice, which makes the prevention of fatigue fractures a vital aspect of the design of machines, vehicles and structures that are subject to repeated loads or vibrations.

Shape of loading	Type of structural component
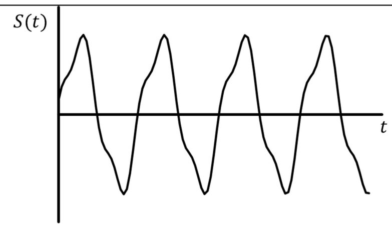	Simple mechanism
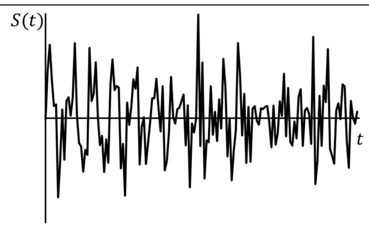	Rigid bridge decks tides winds
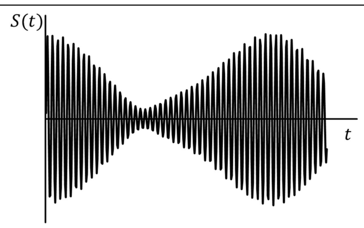	Overhead Conductor

Figure 1: Some typical loading stories acting on structural components.

Fatigue life prediction models of components subjected to random loading are divided into time domain methods and the frequency domain methods. Life prediction methods in the time domain are generally based on identification and cycle counting algorithms associated with a damage accumulation rule. The frequency domain methods, on the other hand, use the spectral density of the loading to estimate the amplitude distribution of the cycles present in the history. In particular, in this work will be discussed and presented the approaches of modeling of fa say that consider that the phenomenon of fatigue is controlled only by stress, that is, characterized by the presence of plastic deformations only at the level of grain (minimum level).

2 Loadings histories and their classifications

In general, loading histories can be classified as **deterministic and non deterministic or random loadings**. Deterministic loading histories are those that can be described by an explicit mathematical relationship. A classic example is the oscillation of a mass-spring system composed of an ideal spring, of elastic constant, attached to a mass body (see Fig. 2).

If the body is moved from its equilibrium position by a distance X and released at time $t = 0$, from basic laws of mechanics or through repeated observations, it can be established that the following relationship between the body's position and the time t.

$$x(t) = X \cos\left(\sqrt{\frac{k}{m}}\right) \tag{1}$$

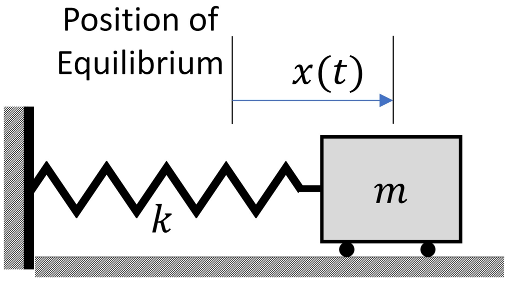

Figure 2: Single spring mass system.

Thus, once the initial offset is X defined, the Eq. (1)Sets the exact location of the body at any time in the future. Therefore, the information representing the mass movement is deterministic.

In other physical systems, there is no functional relationship that allows explaining the behavior of the data that characterizes the behavior of the system (There is no way to predict the exact value of the parameter in a future instant). In these situations, the system is called nondeterministic. In such cases the data are random in nature and should be described in terms of probability of occurrence and/or statistical means, rather than explicit equations. Examples of non-deterministic systems are i) the height of waves in a sea, ii) the dynamic pressure applied on a structure at a specific time instant, iii) the displacement of an automotive suspension system subject to the iterations between the tire and the tread.

2.1 Deterministic histories

Deterministic histories can be classified as periodic or non-periodic. Periodic histories can be further classified as:

- Sinusoidal;
- Complex periodic;
- Quasi-periodic;
- Transients.

2.1.1 Sinusoidal Histories

The histories sinusoidal are histories that can be described by a mathematical function that describes a smooth repetitive oscillation, defined to mathematically by a variable function in the time of the form:

$$x(t) = X \sin(2\pi f t + \theta) \tag{2}$$

where X, f and θ represents, respectively, the amplitude of history, frequency (in Hertz), and the initial phase angle in relation to the origin of time (in radians).

Note that the sinusoidal function belongs to a class of functions called periodic. Periodic functions are those in which the values of the function ($x(t) = y$) are repeated for certain values of the variable t, that is, for each given period, T, we will obtain repeated values for the function, such that:$y = x(t) = x(t + T) = x(t + 2T) = x(t + nT)$ (where T is the repetition period of y and n is an integer).

2.1.2 Complex Periodic Histories

There are per-iodic loading histories that need to be defined mathematically by a variable function in time more complex than that presented in Eq. (2). With few exceptions, these histories (called complex periodic histories) can be expanded into a Fourier series according to the following formula:

$$x(t) = \frac{a_0}{2} + \sum_{(n=1)}^{\infty} \left(a_n \cos(\omega_n t) + b_n \sin(\omega_n t)\right) \tag{3}$$

where a_0, a_n and b_n are called Fourier coefficients, obtained by the expressions:

$$a_0 = \frac{1}{T} \int_0^T x(t)dt \tag{4}$$

$$a_n = \frac{2}{T} \int_0^T x(t) \cos(\omega_n t)dt \tag{5}$$

$$b_n = \frac{2}{T} \int_0^T x(t) \sin(\omega_n t)dt \tag{6}$$

where $n = 1, 2, 3, 4, \ldots$

where $\omega_n = 2\pi f_n$ for $n = 1$, $f_n = f$ is a fundamental frequency.

Considering that x(t) is real, the Eq. (3) can be written as follows:

$$x(t) = X_0 + \sum_{(n=1)}^{\infty} \left(X_n \cos(\omega_n t + \theta_n)\right) \tag{7}$$

where:

$$X_0 = \frac{a_0}{2} \tag{8}$$

$$X_n = \sqrt{{a_n}^2 + {b_n}^2} \tag{9}$$

$$\theta_n = \tan^{-1}\left(\frac{-b_n}{a_n}\right) \tag{10}$$

The identification of harmonic components present in complex periodic histories is very convenient because it allows the graphic representation of these histories through a graph, called frequency spectrum, which correlates the frequencies, and the respective amplitudes present in the loading history.

Example 2.1 Determine the coefficients of the Periodic Signal Fourier Series, $\boldsymbol{x(t)}$, and present the loading history and frequency spectrum of the signal

$$x(t) = x_1 \sin(2\pi f_1 t) + x_2 \sin(2\pi f_2 t) + x_3 \sin(2\pi f_3 t)$$

where $[x_1, x_2, x_3] = [10, 5, 2]e[f_1, f_2, f_3] = [\sqrt{3}, 18, 25]$.

Solution:

Assuming $f = 1$,$T = 1s$ and solving the equations Eq. (5) and Eq. (6) for n ranging from 1 to 30, we found the values represented in Figure 2. 2(a) pp ara the coefficients a_n and b_n. The graphs describing the loading history and frequency spectrum of the signal are shown in figures Fig. 3(b) and Fig. 3(c), respectively.

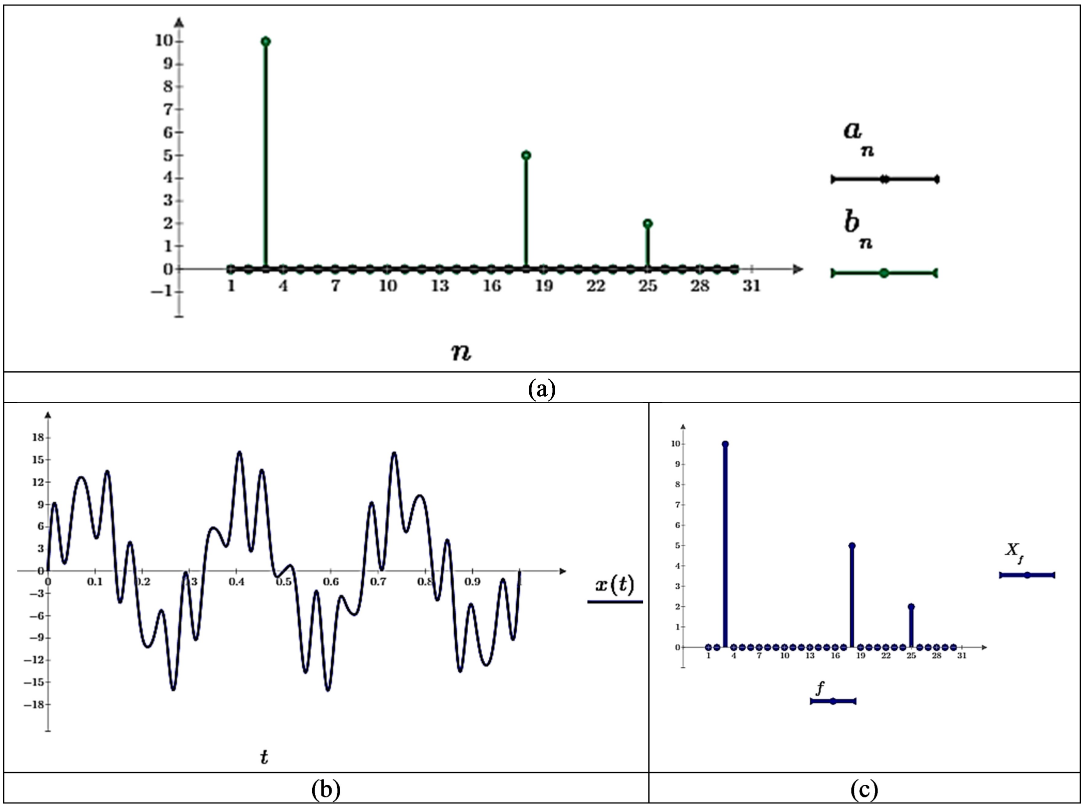

Figure 3: (a) Coefficients and the Fourier series a_n and b_n, (b) representation of history $x(t)$, and (c) representation of the frequency spectrum of history

2.1.3 Quasi-periodic Histories

The sum of two or more sine waves is periodic only when the ratio between all possible frequency pairs are rational numbers. This indicates that there is a fundamental period that will satisfy the periodicity requirement, i.e $x(t) = (t + nT)$. For example, considering the frequencies used in **Example 2.1**, ($[f_1, f_2, f_3] = [\sqrt{3}, 18, 25]$), it is observed that the ratios f_2/f_1 and f_3/f_1 are rational numbers (indicating that the story is periodic!!). However, in some situations the loading history can be composed of frequency components that belong to the set of irrational numbers (i.e., numbers that cannot be represented as a fraction). In these specific situations, the fundamental period is infinitely long and, as a consequence, the resulting time history will not meet the basic requirement of periodicity. When we analyze quasi-periodic histories using the Fourier series, the differences are observed: a a) the frequencies of the components are not related by rational numbers (i.e., the frequencies observed in the frequency spectrum are approximations of the real values), and b) spurious frequency components may appear around frequencies present in the signal, as illustrated in Fig. 4.

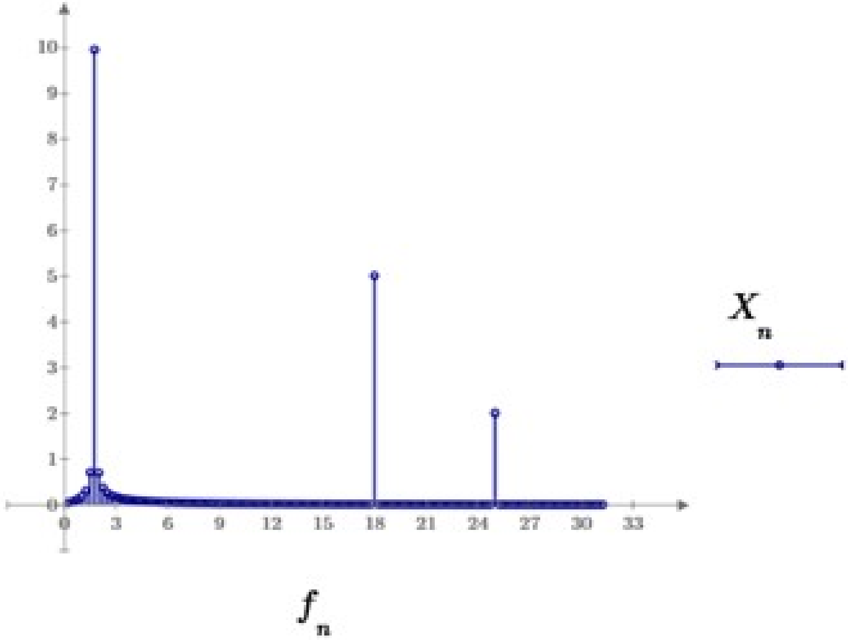

Figure 4: Representation of the frequency spectrum of history of Example 1.

2.1.4 Transient Histories

Determinist histories to transients usually reflect unique events that do not have apparent periodicity, that is, they have no characteristic period. The vibratory response of a mass-spring-damper system resulting from an initial condition $v(t = 0) = v_0 \neq 0$ ou $x(t, = 0) = X_0 \neq 0$, can be given by the expression:

$$x(t) = X_0 e^{-\alpha t} \cos(2\pi f t + \theta) \tag{11}$$

2.2 Stochastic Histories

Stochastic (or random) stories represent physical phenomena that vary to some degree, unpredictably, as time passes, and cannot be described by explicit mathematical relationships because each observation of the phenomenon will be unique. Thus, one can understand a random history as a random variable sequence defined in a probability space. Thus, one can understand a random history as a random variable sequence defined in a probability space. Thus, a single sample representing the observed record over a finite time interval of a random phenomenon is defined as a sample function (represented by each graph of Fig. 5). The collection of all possible sample functions that the random phenomenon may have produced is called a random process or stochastic process (represented by all graphs of Fig. 5). Thus, we can admit that a record observed in a finite time interval of a random phenomenon can be considered as a physical realization of a random process.

Similar to what was observed for deterministic histories, random histories also show differences in terms of their behavior in terms of time. In this sense, the random histories can be classified as stationary or nonstationary.

Conceptually, a time series is said to be stationary when its statistical characteristics (mean, variance, autocorrelation, probability distribution, statistical moments, etc.) are constant over time.

That is, it is a series that develops randomly in time, around a constant mean, reflecting that the probability laws that act in the process do not change over time. Note that for the characterization of a history as stationary is extremely restrictive. For this reason, the definition of this concept takes two forms, namely: a) stationary in the strict sense and b) stationary in the wide sense.

2.2.1 Stationarity in the strict sense (or strongly stationary)

The stochastic process $x(t)$ is said stationary in the strict sense if its statistical properties are invariant to any translation of the origin of the times. This means that processes $X(t)$ and $X(t+\tau)$ have the same statistics whatever the time shift $\Delta\tau$. Formally this means that the joint distribution function obeys equality when it k tends to infinity:

$$F_{X(t_1),X(t_2),\ldots,X(t_k)}(X_1, X_2, \ldots, X_k) = F_{X(t_1+\tau),X(t_2+\tau),\ldots,X(t_k)+\tau}(X_1, X_2, \ldots, X_k) \quad (12)$$

for any temporal translation, any and all instant choice $t_1 < t_2 < \ldots < t_k$.

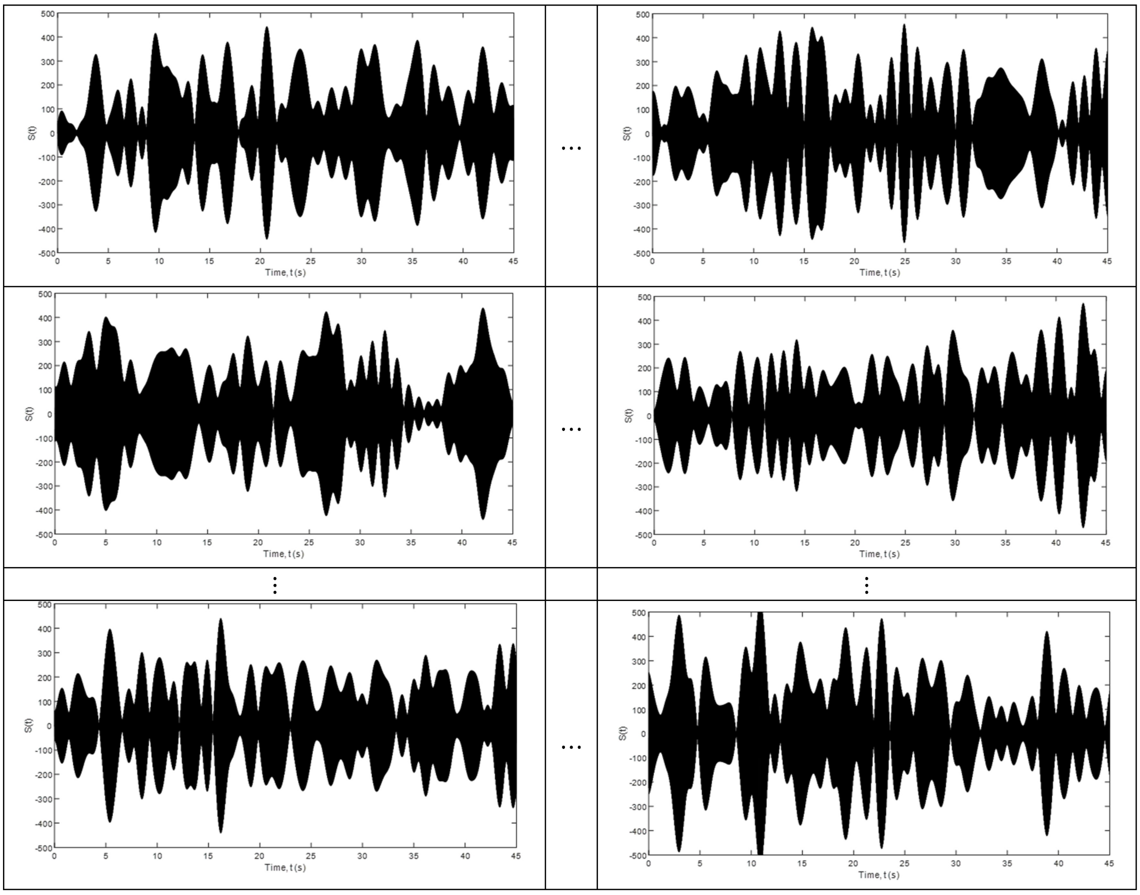

Figure 5: Representation of sample functions of a random process (collection of all possible sample functions).

Figure 2.5 illustrates a set with n sample functions that form a random process. In this figure can be observed the set formed by the realization observed in the moments $t([X_t^1, X_t^2, \ldots, X_t^k])$ and $t+\tau([X_{t+\tau}^1, X_{t+\tau}^2, \ldots, X_{t+\tau}^k])$.

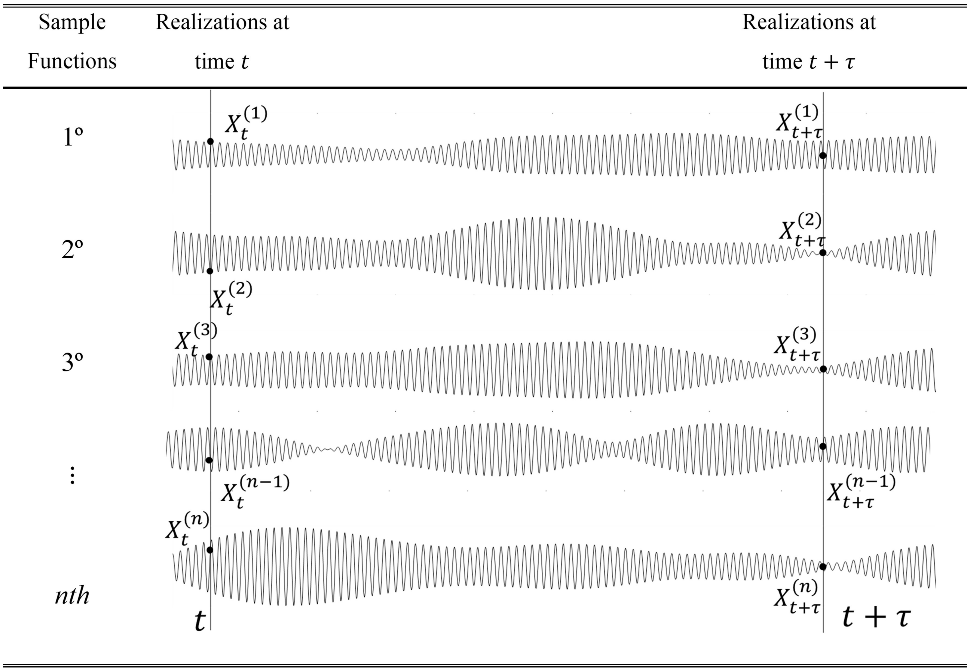

Figure 6: Schematic representation of the acquisition process of the points used to estimate the function of joint distribution of the history observed in two distinct moments of time.

From these two sets of points, you can infer about the behavior of these set of points. For example, the mean value (first-order statistical moment) of the random process at some time t can be calculated by estimating the instantaneous value of each sample function of the ensemble at that particular instant (i.e., the realizations at t), summing the values and dividing by the number of sample functions. Similarly, a correlation (set moment) between the values of the random process in the moments t and $t+\tau$, called the autocorrelation function, $R_{xx}(t_1, t_{1+\tau})$ can be estimated considering the equation Eq. (13):

$$R_x x(t, t+\tau) = \lim_{N\to\infty} \frac{1}{N} \sum_{n=1}^{N} X_t^n X_{t+\tau}^n \tag{13}$$

where τ represents the time interval separating the time series realizations.

When the history is discretized, τ it is calculated as $r\Delta t$ where Δt represents the time interval used to sample the history realizations, and r is called lag and represents the number of time periods separating the time series data (The maximum number of lags, as suggested by Box and Jenkins, is approximately $N/4$ for a history with less than 240 realizations or the largest integer greater than $\sqrt{N}+45$ for a series of more than 240 observations, where N is the number of realizations). Note that when τ it equals zero to Eq. (13) takes the form of the variance estimator.

2.2.2 Stationarity in the wide sense (or weakly stationary)

A less rigorous way of defining the concept of stationarity is known as weak stationarity, stationarity in the wide sense, or covariance stationarity. The random histories that fall as weakly stationary require only that the first moment (i.e., the mean) be constant over time and that the function of autocorrelation, $R_x x(t_1, t_1+\tau)$, (estimated according to the Eq. (13) depends only on τ.

2.2.3 Stationarity of n-order

In some practical situations (for example in fatigue analysis), ensuring that a history is stationary in a wide sense is not enough to perform an adequate modeling of the problem. In these cases, it is interesting to check which moments. In these cases, it is interesting to verify which statistical moments do not change over time, that is, to evaluate the value n of which the Equation satisfies Eq. (12)). In summary, we can conclude that for any random process $X(t)$ where the mean, $\mu(t_1)$, and the autocorrelation function, $R_x x(t_1, t_1 + \tau)$, vary with time t_1, the random process X(t) is said to be nonstationary. For the special case where $\mu(t_1)$ and $R_x x(t_1, t_1 + \tau)$ do not vary as time t_1 varies, the random process $X(t)$ is said to be weakly stationary or stationary in the wide sense. For weakly stationary random processes, the mean value is a constant, and the autocorrelation function depends only on the lag, τ. That is, $(t_1) = \mu_x$ and $R_x x(t_1, t_1 + \tau) = R_x x(\tau)$.

Example 2.2 Determine the auto-correlation functions of the sample functions presented in Fig. 7

Development:

For the history, the outputs of the sample functions were organized in the form of a data matrix DADOS(IxJ) with 1379 (3/0.002175) rows and 17 columns.

Considering that the data are discretized, the estimation of the autocorrelation function is performed using the routine presented in Table 1.

Table 1 – Script MATLAB: function used for calculating the autocorrelation function

```
function [R,t_lag] = AUTO_CORR_M(DATA,LAG,delta_t)
[I J] = size(DADOS);
 for layer=1:LAYER+1
      team = team -1;
       t_lag(law) = (law)*delta_t;
      SAMPLES = I-lag;
      DUMMY = 0;
      for i =1: I-layer
         D1 = DATA(i,:);
         D2 = DATA (i+lag,:);
         D1_D2 = D1*D2';
         DUMMY = DUMMY + (D1_D2);
      end
      R_1(team+1.1) = DUMMY/(J*(I-team));
end
MAX = max(R_1);
R_1 = R_1 /MAX;
end
```

For each history, 17 sample functions of the recorded for 3s are available at a 0.002175s sampling rate.

The routine has as output parameters the vectors t_{lag} (which contains the time intervals that separate the achievements from the time series) and R (which contains the estimate of the history self-correlation function), and as input parameter: a) the data matrix (DATA), b) maximum number of lags (LAG), and the sampling rate (delta_t). As a result of data processing, the auto-correlation functions presented in Fig. 8 are estimated.

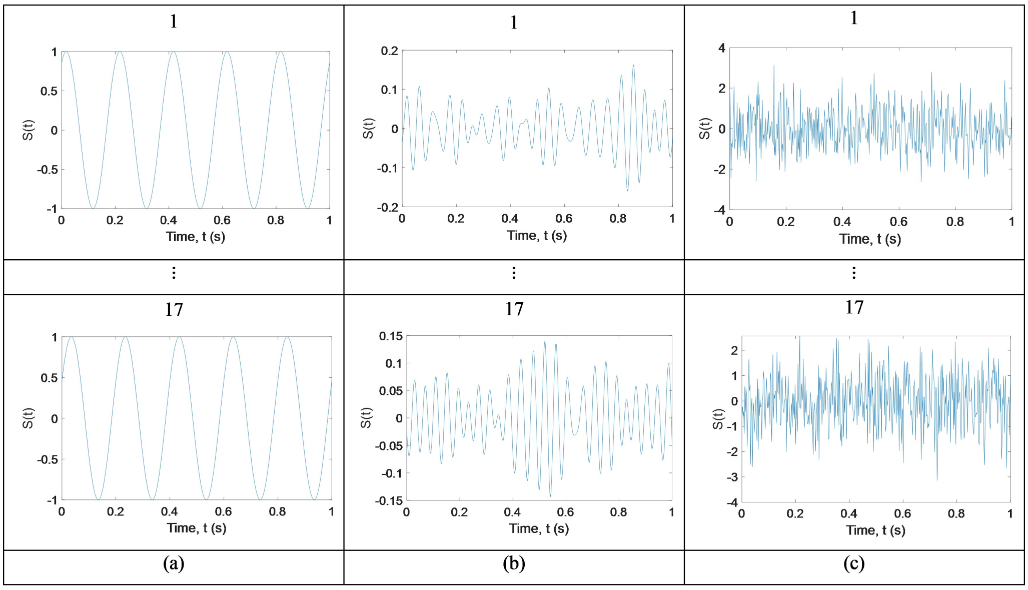

Figure 7: Histories (a) sinusoidal, (b) Narrowband and (c) Noise.

Looking at the charts of Fig. 8 It is verified that the function of autocorrelation of sine history is also a sinusoidal function, which indicates that the correlation between achievements varies cyclically as a function of lag. The function of autocorrelation of the narrow band history (to be defined in following topics) presents a large peak Lag 0 ($R_{xx}(\tau = 0) = Var[S(t)]$) in the followed by a decreasing wave that alternates between positive and negative values, indicating that the correlation between achievements is very strong for when they are very close and weaken as they move away. On the other hand, the function of noise autocorrelation also has a high value in the first or second lag, followed by correlations that are not significant, indicating a strong statistical independence between the achievements of the process.

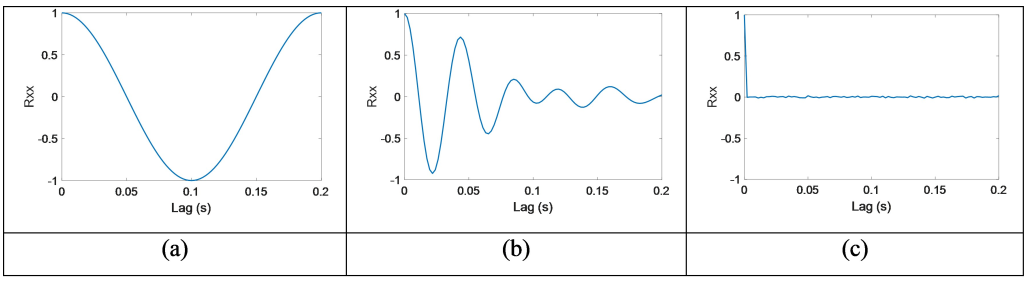

Figure 8: Function of Autocorrelation of histories (a) sine. (b) Complex Periodic, (c) Noisy

Ergodicity

Ergodicity is an important property of a stochastic process, related to stationarity. A process is defined as ergodic in relation to a statistical parameter, if the parameter characterized over time considering a randomly selected sample function is equivalent to the same parameter characterized in the whole set of sample functions in a given period of time. For example, a process is said to be ergodic on the mean if the mean of a randomly selected sample function is equal to the mean of the process over the entire set at any time t or, in other words, if the time mean is the same as the mean of the sample function. Certain statistical conditions must be satisfied to determine whether a process has the property of ergodicity. For example, considering measurements taken over a period T of various sample functions of the process $X(t)$ and assuming that N represents the total number of sample functions, M total number of realizations taken on each sample function over of a period T, and $x_m^{(}(n))$ is the value of the mth realization of the N-th sample function, we can define:

A - Process Ergodic on Average (or ergodic for the First Moment)

If the mean of the sample function (Ensemble average) approaching the mean over time (time average), we characterize this random process as "process ergodic in the mean".

Where the mean of the sample functions at time t_i, $\hat{\mu}_{(X(t_i)}$), is estimated by averaging the n points of the sample functions, that is:

$$\hat{\mu}_{X(t_m)} = \frac{1}{N}\sum_{n=1}^{N} x_i^m \tag{14}$$

and the mean over time is called the *time average* and is estimated by Eq. (15):

$$\hat{\mu}_m^n = \frac{1}{M}\sum_{m=1}^{M} x_m^n \tag{15}$$

B - Ergodic Process in relation to Autocorrelation Function (or Ergodic for the Second Moment)

A process is ergodic in relation to the autocorrelation function if the autocorrelation function of the sample function (*Ensemble autocorrelation*), calculated using Eq. (13) approach the *temporal autocorrelation function* $R_X^j(\tau)$, estimated using Eq. (16).

$$\hat{\mu}_m^n = \frac{1}{M}\sum_{m=1}^{M} x_m^n \tag{16}$$

In more general situations, one is not interested in all the ensemble statistics of a random process. Typically, it is only necessary to guarantee the mean and autocorrelation function (which represents the definition of ergodicity in a more limited sense). In fatigue analysis, to the best of our knowledge, we are also not interested in all ensemble statistics, but in order to be able to use a single sample function to predict fatigue life, we need to ensure that there is ergodicity with respect to the 4th statistical moment.

Example 2.3 Evaluate whether the random process representing a random phase sine wave, represented by the function presented in Eq. (17), is ergodic in relation to the autocorrelation function.

$$s(t) = A\sin\left(2\pi f t + \phi\right) \tag{17}$$

where A is the amplitude of the wave ($A = 10$), f is the frequency, t is the time, and ϕ is the random phase with uniform distribution between 0 and 2π.

Solution:

To answer this question, we will generate a set of sample functions using the routine presented in Table 2. The Fig. 9 shows a set of sample functions generated from the routine described in Table 2.

Table 2 – Script MATLAB: routine for the generation of sample functions representative of a sine wave with random phase

```
J=200; % J defines the number of sample functions
f = 10; %f is the frequency
T=5/f; %T is the observation time (in this case 5 wavelengths will be analyzed
N=10000; %N is the number of points used to describe each sample function
dt = T/N; %dt is the sampling rate
a = 2*pi*f; %a is the argument of the periodic function
phi = 2*pi*rand(J,1); %phi represents a vector containing the J random phases

%time vector calculation
for n =1:N
   t(n,1) = (n-1)*dt;
end
% calculation of nxj matrix containing sample functions
for j=1:J
  for n =1:N
    s(n,j) = 10*sin(a*t(n,1)+phi(j,1));
  end
end
```

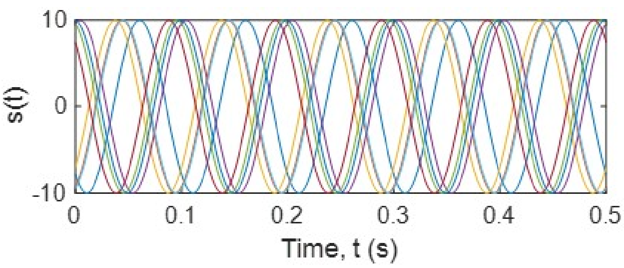

Figure 9: Sine wave sampling functions with random phase.

Once the matrix containing the sample functions is generated, the AUTO_CORR_M function is used to estimate both the autocorrelation function of the sample function (vector R) and the estimates for the temporal autocorrelation function (vector R_t). As a result, the graphs presented in Fig. 10 showed the evolution of the autocorrelation function with the lag time were obtained.

Comparing the estimates of the autocorrelation function of the sample function and the temporal autocorrelation function, it is verified that both have the same behavior. This indicates that random phase sine waves present the characteristic of and ergodicity in relation to the autocorrelation function.

Table 3 – Script MATLAB: AUTO_CORR_M

```
function [R_t, R,t_lag] = AUTO_CORR_M(DATA,LAG,delta_t)
[I J] = size(DATA); %returns the number of rows, I, and the number of columns, J, of the Data array
%Estimation of the matrix containing the temporal autocorrelation functions of each %sample function
for j = 1:J
  for layer=1:LAYER
     t_lag(team) = (team-1)*delta_t;
     team = team -1;
     SAMPLES = I-lag;
     DUMMY = 0;
      for i =1: I-layer
        D1 = DATA(i,j);
        D2 = DATA (i+lag,j);
        D1_D2 = D1*D2;
        DUMMY = DUMMY +(D1_D2);
     end
     R(lag+1,j) = DUMMY/SAMPLES;
   end
  MAX = max(R(:,j));
  R(:,j) = R(:,j) /MAX;
%Estimate of vector containing the estimate of the autocorrelation function of the sample function
 for layer=1:LAYER
     team = team -1;
     SAMPLES = I-lag;
     DUMMY = 0;
      for i =1: I-layer
        D1 = DATA(i,:);
        D2 = DATA (i+lag,:);
        D1_D2 = D1*D2';
        DUMMY = DUMMY +(D1_D2);
     end
     R_1(team+1.1) = DUMMY/(J*(I-team));
end
MAX = max(R_1);
R_1 = R_1 /MAX;
end
```

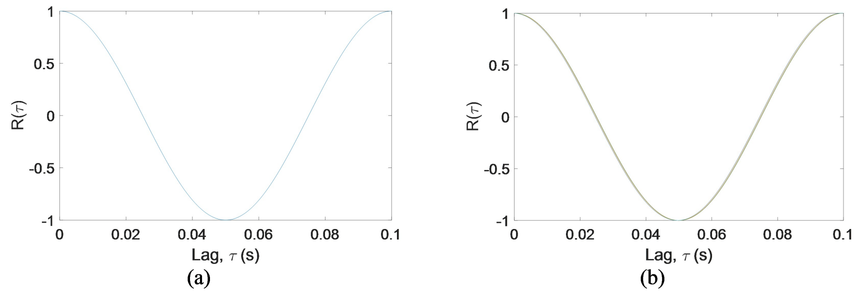

Figure 10: Graphs showing the estimates of (a) autocorrelation function of sample functions and (b) temporal autocorrelation functions.

2.2.4 Non-Stationary Loadings

When random processes cannot be framed as stationary, we say that they are nonstationary. Formally a process is assumed to be nonstationary when the mean and/or variance vary with time. Nonstationary behavior is characterized by the exclusive or combined presence of the following components:

- **Trend**: The *trend* of a random process indicates its "long-term" behavior, that is, whether it grows, decreases or remains stable, and how fast these changes are. For example, increased vibratory response of a system due to increased unbalance, or loss of effectiveness of a damper, etc.
- **Cycles**: *Cycles* are characterized by the oscillations of ascent and fall in the series, smoothly and repeatedly, along the trend component. For example, tidal cycles, winds, operational cycles of equipment.
- **Random walking**: The *random walk* is a statistical phenomenon in which a variable does not follow a discernible trend and apparently moves randomly. The Brownian movement is a classic example of random walking.

In aerospace, automotive and offshore structures, for example, a strategy widely used in the characterization of the loadings (typically non-stationary), consists of modeling tais process s as a sequence of independent modes of operation that occur during a certain period of time. That is, the loads acting on these structures can be described as a sequence of stationary processes. For example, when analyzing the forces acting on an aircraft, it is common to divide the flight stages into a sequence of loading histories related to the flight phases/conditions/aircraft type (e.g. taxi, takeoff, gusts, cruise, maneuver , landing). Fig. 11 shows a sketch illustrating a typical loading history of aircraft transport aircraft.

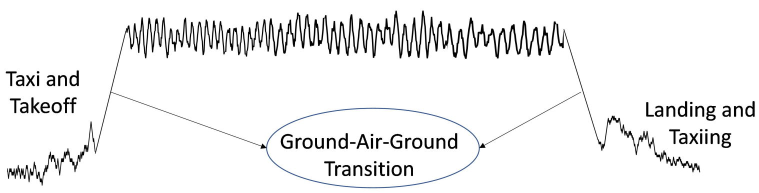

Figure 11: Schematic representation of a typical history of carrying aircraft loading.

3 Fatigue of Materials: Introduction to Stress-Based Approach

As discussed in the previous chapter, during their useful lives it is very likely that structural components are subject to cyclic loads. These loads can have a constant amplitude or amplitude that varies over time. Regardless of the type of load applied, there are three main approaches to analyze and project against fatigue failures. The traditional stress-based approach was developed essentially to its current form in 1955. In this approach, the analysis is based on nominal stresses working at the critical points of the component. The nominal stress that can be applied under cyclic load is determined considering the average stresses and adjusting the effects of stress increases (due to the presence of stress concentrators). Another approach is the deformation-based approach, which involves a more detailed analysis of localized flow that can occur at critical points during cyclic loading. Finally, there is the approach of fracture mechanics, which specifically treats the increasing cracks by the methods of fracture mechanics.

Whereas the service lives of real structures are relatively long (*High number of cycles to failure*),that the stress levels are lower than the material flow stress (*little plastic deformation due to cyclic loading*), and due to the ease of implementation, the stress-based approach is the most traditional and most frequently used in applications involving fatigue under random conditions. This approach assumes that the amplitude of the stress acting at the critical point is responsible for the process of initiation and propagation of fatigue cracks and that fatigue life, expressed in terms of the number of load cycles, is a direct function of the intensity of the stress amplitude.

The stress-based method has its origins in the investigations carried out by August Wöhler in 1858 and resulted in the widely known Wöhler curve, or S-N curve (i.e. stress, S, versus number of cycles for failure, N).

The simplest way to characterize the fatigue behavior of a material is to subject standardized specimens to efforts with sinusoidal characteristics with prescribed amplitudes (with zero mean) and count the number of cycles or stress inversions necessary for complete rupture of the specimen. From the experimental results, one S-N diagram (called diagram or Wöhler diagram) is constructed, which displays very conveniently the basic fatigue data in the elastic stress range (fatigue under high cycle conditions) on a graph that correlates the amplitude of the actuating stress (S_a) versus number of cycles until failure (N).

The S-N diagram covers a life range ranging from 1 cycle to a very high number of cycles. Due to the different physical phenomena that may be related to the fatigue process, it is observed that the relationship between stress and life presents different behaviors for different life ranges. For this reason, as illustrated in Fig. 12, the S-N diagram is usually divided into three regions: (i) low-cycle fatigue (LCF) for life lower than 103 cycles, (ii) high cycle fatigue (HCF) for life up to 107 cycles, and (iii) very high cycle fatigue (VHCF) for cycles greater than 107 (the VHCF region is also called the Giga cycle fatigue region (GCF) for life upper to 10^9 cycles). In general, the region of high-cycle fatigue is located between the two knees observed and the region known as the finite life region begins at the end of the 1st knee and ends at the beginning of the 2nd and then, as shown in Fig. 12. Typically, fatigue analyses using the stress-based approach adopt the relationship between stress and life in the finite life region based on describing fatigue behavior. The analytical representation that describes the behavior of material fatigue in this region is commonly expressed in the form:

$$S = AN^{-b} \tag{18}$$

$$NS_a^{\frac{1}{b}} = k = \left(\frac{1}{A}\right)^{\frac{1}{b}} \tag{19}$$

where b, k and A are material parameters estimated from test data obtained using identical samples. The basic methodology for characterizing the statistical behavior of these parameters can be found in ASTM E739-10 [2015] - *Standard Practice for Statistical Analysis of Linear or Linearized Stress-Life (S-N) and Strain-Life (ϵ-N) Fatigue Data.*

For ferrous materials in general, it is often adopted a threshold stress amplitude (endurance limit, S_e), below which it is assumed that the material does not fail by fatigue (has infinite life). For engineering purposes, this infinite life is generally regarded as cycles. 10^6 Assuming the existence of endurance limit, the relationship S-N takes the following form:

$$N = \begin{cases} N = AS^{-b}, & S_a > S_e \\ \infty, & S_a \leq S_e \end{cases} \tag{20}$$

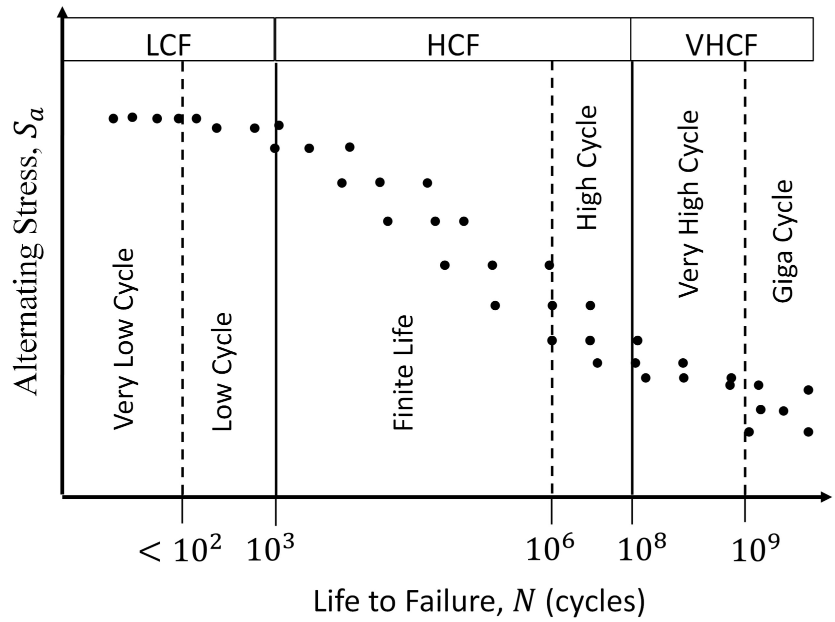

Figure 12: Schematic representation of the S-N diagram.

3.1 Mean Stress Effect

Stress amplitude strongly influences the fatigue behavior of a structural component. However, the presence of an average component in the loading history is also important, as a secondary way) in the characterization of fatigue behavior.

In general, the characterization of the mean stress effect on fatigue behavior, the S-N diagrams should be constructed considering that the experimental points are performed under constant mean stress conditions. Another procedure often used in the construction of the S-N diagram that represents the effect of the mean stress is to use test results performed under stress ratio conditions, constant $R = \sigma_{min}/\sigma_{max}$.

A very usual way of representing the effect of the mean stress on the fatigue behavior is through the Haigh diagram (or constant life diagram). This diagram allows the identification of alternating stress pairs, S_a, and mean, S_m, responsible for fatigue failure after the application of N load cycles. The ordinate of the Haigh diagram represents the stress amplitude, S_a, normalized by the fatigue limit, S_e, and the abscissa represents the mean stress normalized by the ultimate tensile strength, S_u (see Fig. 13). In theory, the curve that best fits the experimental data represents the combinations between S_a and S_m responsible for fatigue failure after N cycles. Since the tests required to generate a Haigh diagram is expensive and do not allow one to obtain a curve that represents the typical behavior of the material (since the fitted curve will always depend on the quality of the experimental data), several empirical relations have been developed to generate the curve that defines the failure condition for a given life (typically this procedure is used to define the curve that represents the design conditions for infinite life). These methods use various curves to connect the endurance limit on the alternating stress axis to either the yield strength, S_y, ultimate strength, S_u, or true fracture stress, σ_f, on the mean stress axis.

The curve that connects these two points in each of the coordinate axes hypothetically represents the combinations S_a between S_m and responsible for fatigue failure after the application N of loading cycles. Eq. (21) presents a generalized expression to represent empirical relationships widely used to evaluate the effect of mean stress on fatigue behavior:

$$\left(\frac{S_a}{\sigma_f(N)}\right)^n + \left(f\frac{S_m}{S_u}\right)^m = 1 \tag{21}$$

where f, n and m are constants that assume different values according to the empirical relationship considered and S_u represents the tensile strength limit of the material. Without further details, the most adopted criteria can be derived considering the constants presented in Table 3.1.

Table 1: Constants that characterize the empirical relationships used to evaluate the effect of mean stress on fatigue behavior.

Relation	Parameter		
	m	n	f
Geber	2	1	1
Goodman	1	1	1
Morrow	1	1	$S_u/\tilde{\sigma}_{fB}$
Sailor	2	2	1
Dietmann	1	2	1

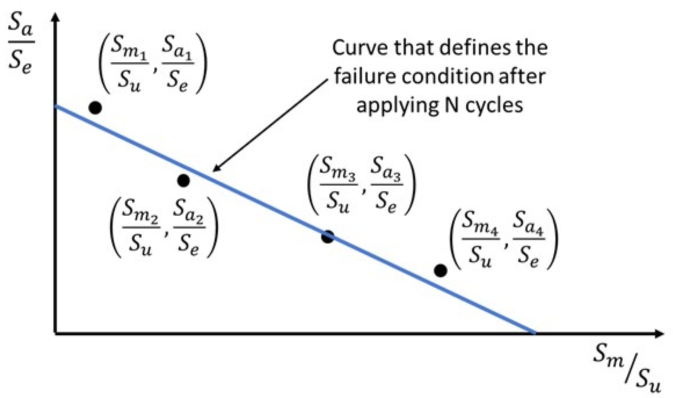

Figure 13: Schematic representation of the Constant-life diagram (Haigh diagram).

3.2 Accumulated Damage Concept and Miner Rule

The fatigue failure process in ductile metals is intrinsically related, at a first stage, to the nucleation of microcracks resulting from the movement of disagreements during cyclic loading. This cyclic movement leads to the appearance of thin steps on the surface (intrusions and extrusions) that act as stress amplifiers where micro cracks start. In a second step of the fatigue process, micro-cracks coalesce and begin to propagate through the material. With the continued cyclic loading, the growth of the cracks progresses until the still intact section of the material can no longer withstand the imposed load and experiences a rapid fracture. All this process of degradation structural can only be monitored and measured in highly controlled laboratory environments. And in practical applications, the estimation of component lifes subject to random loadings is made based on data from fatigue studies performed for constant amplitude loads, and the law of linear damage accumulation proposed by Miner.

In the formulation of the law of accumulation of Miner damage, it is considered that the damage, dinduced by a cycle, nof the stress amplitude S_a is estimated by the following expression:

$$d = \frac{n}{N_f} \tag{22}$$

where N_f it represents the number of cycles required for a periodic load with a constant amplitude equal S_a to induce component failure in the structure.

Considering the history of stresses is composed K of stress amplitude classes, each being applied times n_k , the Miner rule is written as:

$$d = \sum_{k=1}^{K} d_k = \sum_{k=1}^{K} \frac{n_k}{N_{f_k}} \leq D_c \tag{23}$$

where D it represents the accumulated damage D_c and represents critical damage and must be determined experimentally.

In the absence of further information, it should be assumed that the failure will occur when the critical damage reaches a nominal value of 1,0. However, and all these studies show that the median values of damage observed in specimens at certain loading conditions vary from 0,15 to 1,6.

Example 3.1 A mechanical component was manufactured with steel that has a tensile strength limit, S_u, equal to 755 MPa and a fatigue behavior described by the following Wöhler function $S_a = 1440N^{(-0.096)}$. Under operating conditions, the stresses at the critical point of this component are applied in the form of a sequence of loading blocks with constant amplitudes, as shown in Fig. 14. Considering this information, time out the number of load blocks that can be applied until the component fails.

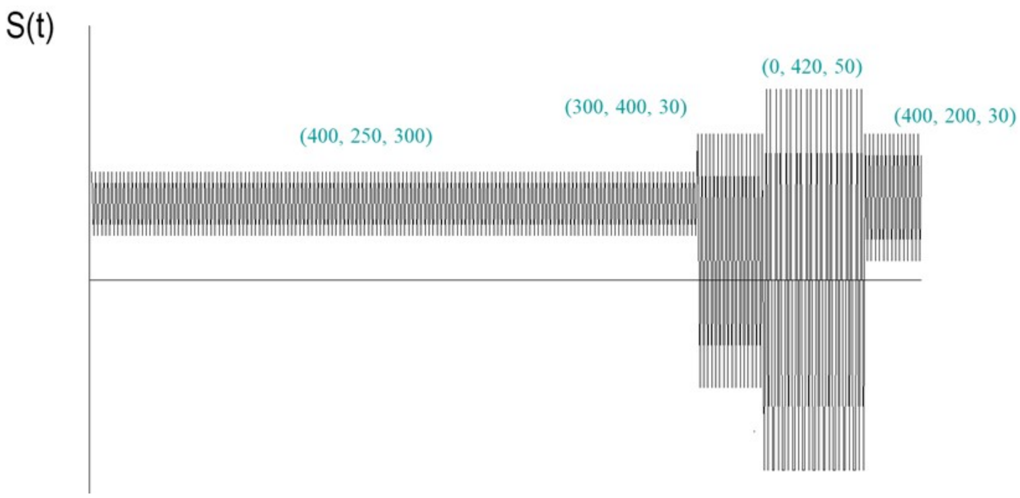

Figure 14: Sequences of block loading.

Solution:

Characteristics of the sinusoidal loading sequence S_m,S_a,n):

(1) (400, 250, 300);

(2) (300, 400, 30);

(3) (0, 420, 50);

(4) (400, 200, 30).

The estimate of the damage accumulated by this loading block will be performed considering Eq. (23). For this particular case, the sum of the damage increments will take the following form:

$$D_{block} = \frac{300}{N_f(250, 400)} + \frac{30}{N_f(400, 300)} + \frac{50}{N_f(420, 0)} + \frac{30}{N_f(200, 400)} \tag{24}$$

where N_f (S_a,S_m) represents the number of cycles that could be applied if the pair of alternating stresses, S_a, and average, S_m were applied continuously until the failure of the mechanical component.

Considering, for example, the Goodman ratio the value of N_f will be calculated through the following equation:

$$N_f(S_a, S_m) = \left[\frac{S_a}{A\left(1 - \frac{S_m}{S_u}\right)}\right]^{\frac{1}{b}} = \left[\frac{S_a}{1440\left(1 - \frac{S_m}{755}\right)}\right]^{\frac{1}{-0.0961}} \tag{25}$$

where S_u is the limit of tensile strength, and A and b represent the constant and exponent of the curve of Wöhler.

Substituting the mean and alternating stresses into Eq. (25), one arrives at the results presented in Table 2.

Table 2: Estimation of the damage produced by each constant amplitude load present in the loading block shown in Fig. 14

Event	S_m	S_a	n	$N_f(S_m, S_a)$	d
1	400	250	300	3,18E+04	9,43E-03
2	300	400	30	3,16E+03	9,48E-03
3	0	420	50	3,70E+05	1,35E-04
4	400	200	30	3,24E+05	9,25E-05

As a consequence of the application of a loading block, it is verified that the damage accumulated with each application of this load sequence is equal to 1.91E-3. Assuming that the number of blocks that can be applied is equal to:

$$Num.blocks = \frac{D_c}{D_{blocks}} = \frac{1}{1.91 \cdot 10^{-3}} = 52 \tag{26}$$

4 Random Fatigue Analysis in the time domain

As commented in Section 1 to Section 3, over their useful life, many structural components are subjected to cyclic loads. These loads can be applied under constant amplitude conditions or under amplitude conditions that vary over time. We also show that in situations where structural components are subjected to constant amplitude loads (with or without average component) or in conditions of application of loading blocks with varying amplitudes, the determination of fatigue life is a relatively simple task. However, if the loading amplitude varies at random over time, it is more difficult to characterize a loading cycle and its corresponding amplitude. This difficulty forced fatigue researchers to develop cycle identification and counting methodologies to reduce a complicated loading history in a series of simple and discrete constant amplitude loading events. These methods were initially developed for the study of fatigue damage generated in aeronautical structures and, over the last decades, several counting methods have been proposed, leading to different results and, therefore, to erroneous predictions of fatigue life. However, there was a consensus that the best approach is the procedure called Rainflow, introduced by Endo in the late 1960s, being the first article in English by Matsuichi and Endo [1968]. The procedures for using the Rainflow cycle counting method were standardized together with other counting methods in ASTM ASTM-E1049-85 [2017] Standard Practices for Cycle Counting in Fatigue Analysis.

For the implementation of the rainflow method, it is necessary to initially transform the history of stresses into a sequence of peaks[1] and valleys [2], which represent the points at which the first derivative of the stress history changes sign (note that peaks and valleys are specific definitions for reversals), as illustrated in Fig. 15.

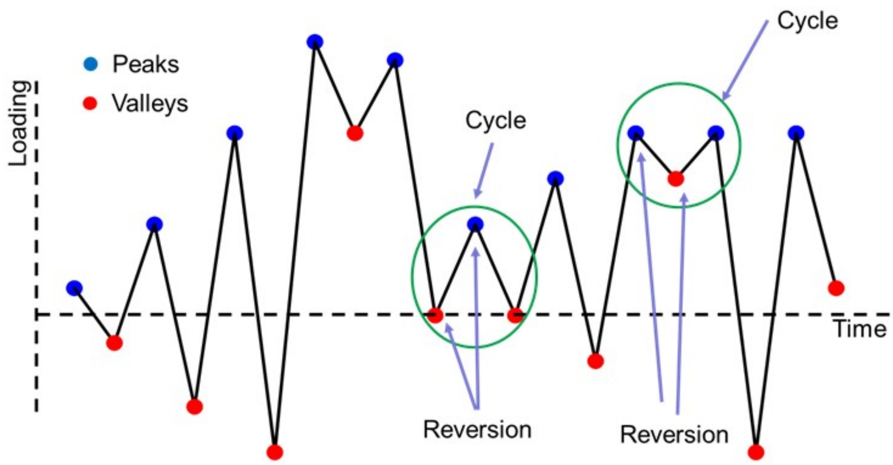

Figure 15: Identification of the basic parameters of a history used by the Rainflow method for the identification and counting of cycles.

From empirical observations of the stress-strain curve estimated from tests under variable amplitude conditions, it is verified that when the material is subjected to a history of stresses or deformations, small load reversals occur appear in the $\sigma - \epsilon$ diagram, but without affecting the large reversals and the response of the material. This behavior is represented in Fig. 16, in which it is observed that the loading sequence 2-3-4 generates the 2-3-2' cycle that does not interfere with

[1]The point at which the first derivative of the load-time history changes from a positive to a negative sign; the point of maximum load in constant amplitude loading.

[2]The point at which the first derivative of the load-time history changes from a negative to a positive sign (also known as trough); the point of minimum load in constant amplitude loading.

the evolution of the 4-5 section. By analogy, the rainflow technique treats the same way the closed stress-strain curves (hysteresis cycles), in which the small reversals of load in a fatigue cycle with greater amplitude will also not interfere with the accumulated damage by fatigue.

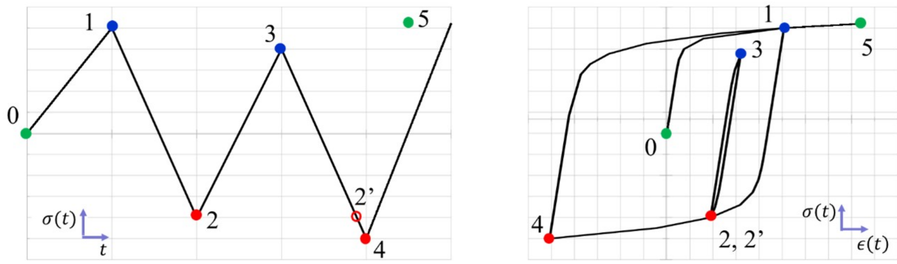

Figure 16: Example of the behavior of the stress-strain curve for a given stress history.

In essence, the Rainflow method identifies reversals and not loading cycles, but as can be seen in Fig. 15 and 16, two segments of equal amplitudes that have a common reversal represent a loading cycle.

A series of rules are used to identify load cycles in the Rainflow method. However, the core of the method of identifying the reversals present in history consists of comparing the bands formed by three consecutive reversals (S_i,S_j,S_k), see Fig. 17. Thus, the three consecutive reversions (S_i,S_j,S_k) are used to define the stress ranges: $R_l = |S_i - S_j|$ (left track) and $R_r = |S_j - S_k|$ (right track). If the left band R_l, is less than or equal to the right band, the R_r material shall be considered to have been subjected to 1 or 1/2 loading cycles with alternating stress, S_a, and mean stress, S_m, calculated by the following expressions:

$$S_a = \frac{R_l}{2} \tag{27}$$

$$S_m = \frac{S_i + S_j}{2} \tag{28}$$

If the condition $R_l \leq R_r$ is not met, it is assumed that the loading (S_i,S_j,S_k) run does not induce loading cycles in the material.

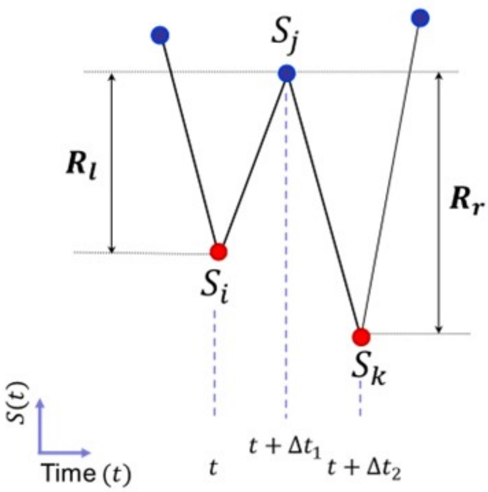

Figure 17: Primal criteria for the identification of a reversal according to the rainflow method.

From the comparison between R_l and R_r, a few more rules are required to implement the Rainflow method.

1. Turn the loading history into a sequence of peaks and valleys, quantify the number of peaks and valleys present in the sequence, L, and set the counter l (at the beginning of the counting process $l = 1$).
2. Define an I×3 matrix in which each row will be stored the information about the alternating stress, S_a, the mean stress, S_m, and the number of reversals, n, identified during the cycle counting process.
3. The count is performed initially from the first position of the peak sequence or valley present in history.
4. If $L > 2$, form the first triple $(S_i, S_j, S_k) = (S_l, S_{(l+1)}, S_{(l+2)})$, $l = 1$.
5. Calculate the tracks R_l and R_r using the reversals (S_i,S_j,S_k) and compare tracks R_l and R_r.

5.1. If $R_l \leq R_r$:

5.1.1. If the reversal S_i is in the first position of the sequence of peaks and valleys ($l = 1$):

5.1.1.1. Calculating S_a and S_m using Eq. (27) and Eq. (28) and transport S_a, S_m and $n = 1$ to the rainflow matrix.

5.1.1.2. Delete point $S_($l=1$)$ from the sequence of peaks and valleys, rearrange it, and make $L = L - 1$.

5.1.1.3. If $L > 2$:

5.1.1.3.1. Form the term (S_i, S_j, S_k)=(S_1, S_2, S_3) and go to Step 5.

5.1.1.4. If $L = 2$:

5.1.1.4.1. Calculating S_a and S_m using Eq. (27) and Eq. (28) and transport S_a, S_m and $n = 1$ reversion to the rainflow matrix.

5.1.1.4.2. End counting process.

5.1.2. If the reversal S_i is not in the first position of the sequence of peaks and valleys ($l \neq 1$):

5.1.2.1. Calculate S_a and S_m using Eq. (27) e Eq. (28) and transport the values of S_a, S_m, $n = 2$ and reversals to the rainflow matrix

5.1.2.2. Delete points S_i and S_j from the sequence, rearrange the sequence, make $L = L - 2$, $l = l - 1$.

5.1.2.3. Form the triple (S_i, S_j, S_k)=($S_l, S_(l + 1), S_(l + 2)$) and go to Step 5.

5.2. If $R_l > R_r$

5.2.1. If $l \leq L - 3$.

5.2.1.1. $l = l + 1$

5.2.1.2. Form the triple (S_i, S_j, S_k) = (S_1, S_2, S_3) and go to Step 4

5.2.2. If $l > L - 3$.

5.2.2.1. Calculate for each remaining range (S_i, S_j) S_a and S_m and transport the values to S_a, S_m and $n = 1$ to the rainflow matrix

5.2.2.2. Finish the counting process.

Example 4.1 Identify the carga cycles present in the stretch of the loading section shown in Fig. 18

Solution:

The Fig. 19 presents the sequence of steps required to implement rainflow count of the history illustrated in Fig. 18, that presents the result of the cycle count by applying the rainflow algorithm to loading.

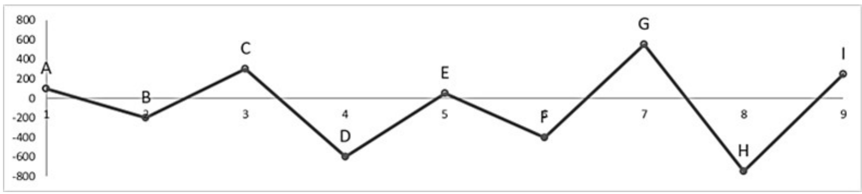

Ponto	Tensão
A	100
B	-200
C	300
D	-600
E	50
F	-400
G	550
H	-750
I	250

Events		Stress		S_a	S_m	n
Start	End	Start	End			
A	B	-2	1	1.5	-0.5	1
B	C	1	-3	2	-1	1
E	F	-1	3	2	1	2
C	D	-3	5	4	1	1
D	G	5	-4	4.5	0.5	1
G	H	-4	4	4	0	1

Figure 18: Example of a service load-time history and the results of the cycle counting

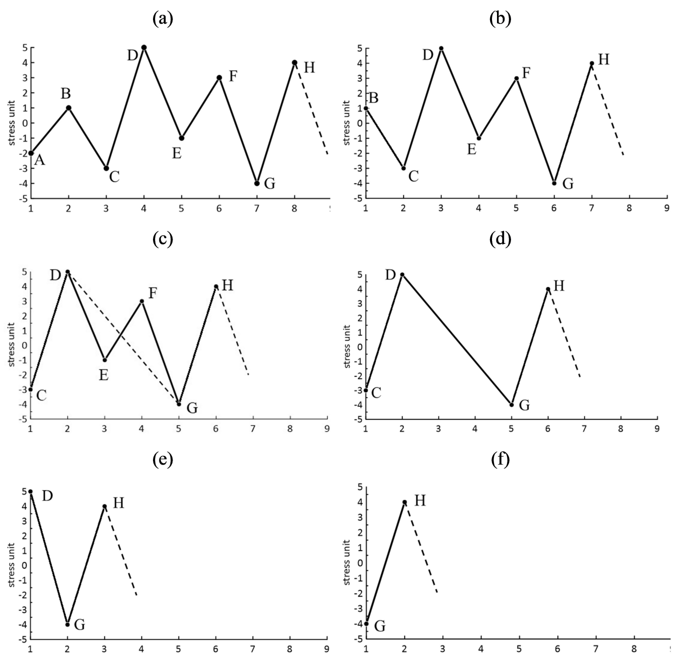

Figure 19: Example 1 of the rainflow counting method using the rules presented in this chapter.

$l = 1$ $N = 9$	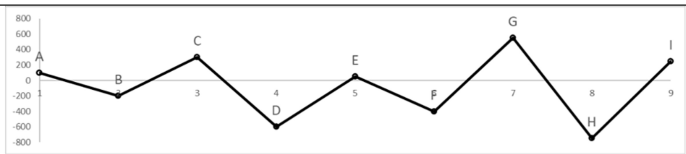	Initial sequence of peaks and valleys, $\boldsymbol{V}$ to form (S_l, S_{l+1}, S_{l+2})
$l = 1$ $N = 9$	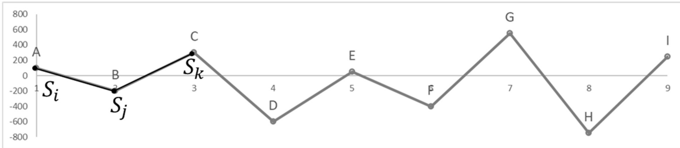	½ cycle identified (Start, End) = (A, B) Discard point(s): A Rearrange $\boldsymbol{V}$ to form (S_l, S_{l+1}, S_{l+2})
$l = 1$ $N = 8$	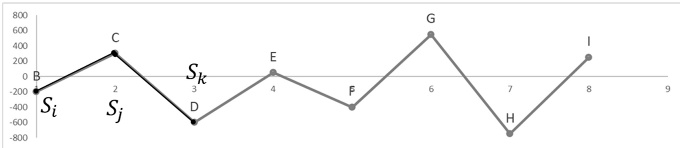	½ cycle identified (Start, End) = (B, C) Discard point(s): B Rearrange $\boldsymbol{V}$ to form (S_l, S_{l+1}, S_{l+2})
$l = 1$ $N = 7$	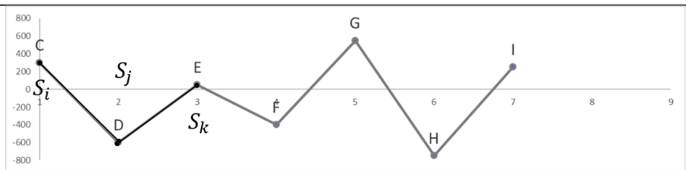	unidentified cycle Advance one position $(l = l + 1)$ to form (S_l, S_{l+1}, S_{l+2})
$l = 2$ $N = 7$	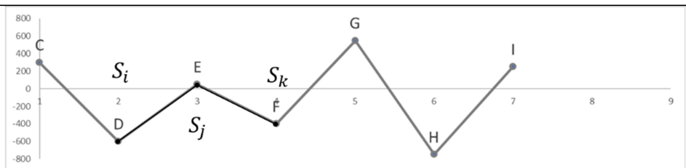	unidentified cycle Advance one position $(l = l + 1)$ to form (S_l, S_{l+1}, S_{l+2})
$l = 3$ $N = 7$	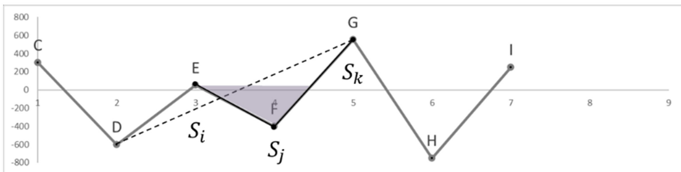	1 cycle identified (Start, End) = (E, F) Discard point(s): E – F Rearrange $\boldsymbol{V}$ $(l = l - 1)$ to form (S_i, S_j, S_k)
$l = 2$ $N = 5$	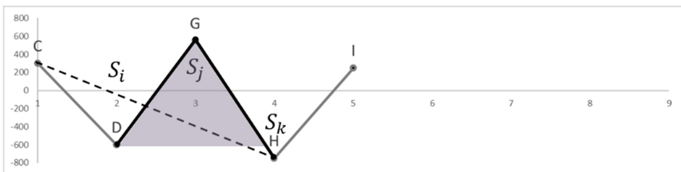	1 cycle identified (Start, End) = (D, G) Discard point(s): D – G Rearrange $\boldsymbol{V}$ $(l = l - 1)$ to form (S_i, S_j, S_k)
$l = 1$ $N = 3$	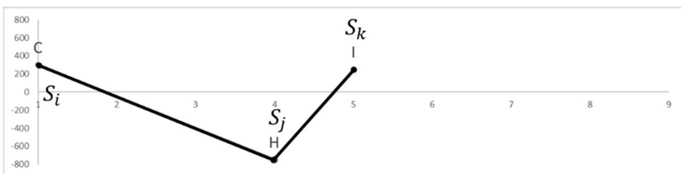	½ cycle identified (Start, End) = (C, H) Discard point(s): C ½ cycle identified (Start, End) = (H, I) Discard point(s): H end of count

Figure 20: Example 2 of the rainflow counting method using the rules presented in this chapter.

5 Random Fatigue Analysis in the Frequency Domain

5.1 Spectral Properties

Fatigue analysis is often performed in the time domain, where all input and output loading, stress response or strain, are time-based signals. In some situations, however, the stress response and input loading are preferably expressed as frequency-based signals, usually in the form of a power spectral density (PSD) graph. In this case, a system function is required to relate a loading input PSD to the response output PSD Lee [2005].

For linear systems, fatigue calculations performed entirely in the frequency domain can shorten the calculation time considerably, which corresponds to the so-called frequency domain approach (Dirlik and Benasciutti [2021])

The PSD represents the energy of the time signal at different frequencies and is another way to denote the charging signal in the time domain. The Fast Fourier Transform (FFT) of a signal in time can be used to obtain the loading PSD, while the Inverse Fourier Transform (IFT) can be used to transform the frequency-based signal for time-based loading. The transformation of the loading history between the time domain and the frequency domain is subject to certain requirements, according to which the signal must be stationary, random, and Gaussian, i.e., not varying its statistical properties over time and presenting normal distribution (Lee [2005]). An ergodic process is a stationary process whose expected value (envelope) statistics are identical to time statistics (Dirlik [1985]).

In practice, a one-sided spectral density, $G(f)$, is often used, limited only to the positive frequency range of the two-sided spectral density, $S(f)$, as negative frequencies have no physical meaning (Bishop [1988]). A random signal can be classified based on its frequency content, i.e., the shape of its PSD. The signal is called narrowband if the PSD peaks around a single frequency, usually the resonant frequency of a vibrating system. In all other cases where the PSD covers a wider range of frequencies, the random signal is termed broadband (Dirlik and Benasciutti [2021]).

Fig. 21 compares sample histories representative of two distinct types of random processes, showing the differences between the time histories based on their corresponding PSD. Power spectra with rectangular blocks were considered which are just idealizations of the smoother spectra typically found in practical applications.

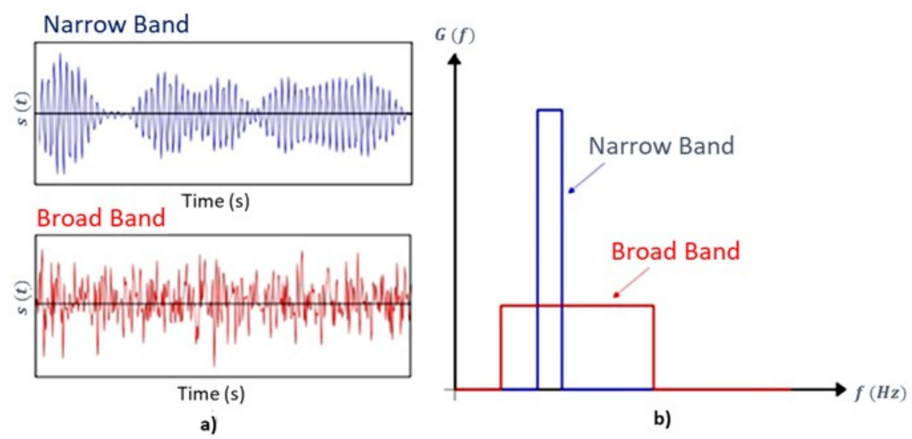

Figure 21: a) Time history samples b) Narrowband and broadband PSD of the history samples.

The narrowband or broadband process is defined by means of several spectral parameters, among them we define the spectral moments of n-order, λ_n, as:

$$\lambda_n = \int_{-\infty}^{+\infty} |f|^n S(f) df = \int_{-\infty}^{+\infty} f^n G(f) df \quad , \quad n = 0, 1, 2, \cdots \tag{29}$$

The zero-order moment, λ_0, can be used as an alternative method of calculating the root mean square (RMS) value, which is a good indication of the intensity of a loading history.

$$RMS = \sigma_S = \sqrt{\lambda_0} \tag{30}$$

and also represents an important feature in the time domain, which is the uniaxial loading history variance $s(t)$:

$$\lambda_0 = \int_{-\infty}^{+\infty} G(f) df = Var(s(t)) \tag{31}$$

From the spectral moments, some spectral characteristics can be calculated, such as the expected rate of zero upcrossings v_0 per unit of time.

$$v_o = \sqrt{\frac{\lambda_2}{\lambda_0}} \tag{32}$$

and the expected level upcrossing rate v_p per unit of time.

$$v_p = \sqrt{\frac{\lambda_4}{\lambda_2}} \tag{33}$$

The irregularity factor will essentially measure how many peaks a signal has for each time the signal crosses at zero stress level (Lee [2005]). The ratio between the zero-crossing rate and the peak-crossing rate is known as the irregularity factor α.

When the irregularity factor tends to one, it means that for each peak, there will be approximately one zero level crossing and the process will have a narrow bandwidth, that is, v_0 is equal to v_p. However, when the bandwidth is wide, it is said that the irregularity factor will tend to zero, thus there will be infinite peaks for each zero-level crossing, characterized by a more irregular process (Lee [2005]).

The irregularity factor, which varies between 0 and 1, can be used to characterize the shape and geometric distribution of the frequency of a given spectrum as a function of spectral moments (Benasciutti and Tovo [2005]). In general, it can be calculated as:

$$\alpha_n = \frac{\lambda_n}{\sqrt{\lambda_0 \lambda_{2n}}} \tag{34}$$

The process is considered narrowband if its spectral density has only a narrow range of frequencies. In contrast, a broadband process is one whose spectral density covers a wide band of frequencies, this bandwidth is called the width parameter (Lee [2005]). The spectral width parameter, γ, is introduced as:

$$\gamma = \sqrt{1 - \alpha^2} \tag{35}$$

Thus, narrowband processes must have an irregularity factor equal to 1 and a width parameter equal to 0, while wideband processes must have an irregularity factor approaching 0 and a spectral width parameter approaching 1 (Lee [2005]).

5.2 Fatigue Damage Based on Power Spectral

For the fatigue life of gaussian and stationary processes, the Miner rule will be used to estimate the fatigue damage per unit time from the amplitude distribution of the stress cycles present in the loading history, $f_{(S_a)}(S_a)$. This is achieved by following the following procedures:

Assume a history of stresses whose amplitudes vary over time, $S(t)$. Through the rainflow counting technique, for example, this variable-amplitude load is transformed into a sequence of constant-amplitude blocks, S_{a_i}. So, using the Palmgren-Miner, the damage D can be estimated through the following equation:

$$D = \sum_{i=1}^{K} \frac{n_i}{N_{f_i}} \tag{36}$$

where n_i is the total number of cycles in the ith block of constant-stress amplitude $\sigma_{a,i}$, N_{f_i} is the number of cycles to failure under $\sigma_{a,i}$, and I is the total number of blocks. Recall that the relationship between constant stress amplitude $\sigma_{a,i}$ (or constant stress range $\sigma_{r,i}$) and the fatigue life N_{f_i} has the following expression:

$$\sigma_{a,i} = AN_{f_i}^{-b} \tag{37}$$

$$N_{f_i}\sigma_{a,i}^{m} = k \tag{38}$$

where A is the fatigue strength coefficient and b is the fatigue strength exponent. If $m = 1/b$, $k = A^m$.

The amplitude distribution of the stress amplitude present in the loading history, $f_{\sigma_a}(\sigma_a)$ can be established performing the rainflow cycle counting technique (see Fig. 22).

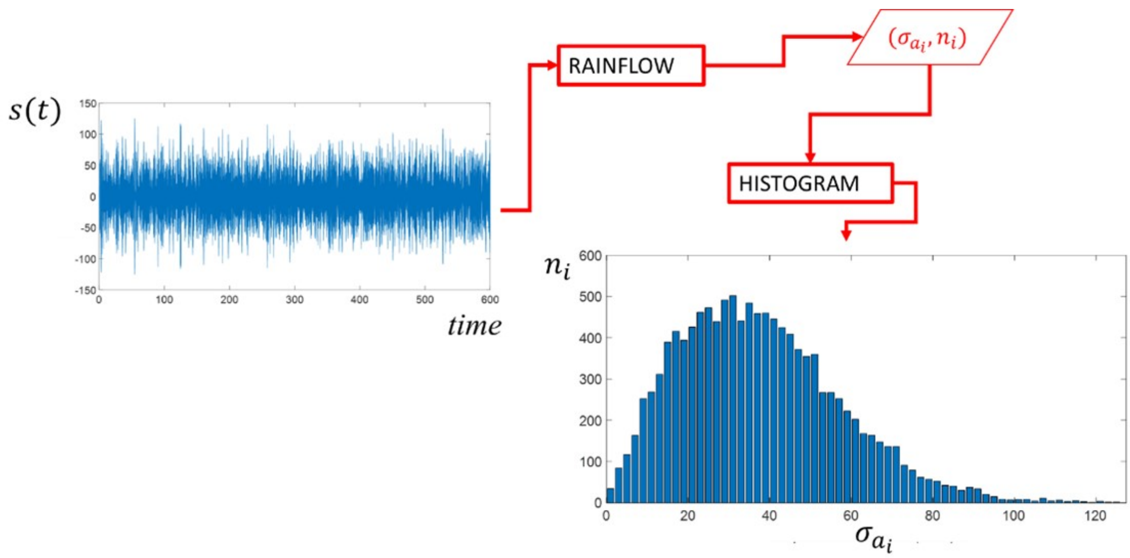

Figure 22: Basic strategy for obtaining the histogram representative of the distribution of stress amplitudes present in a random loading history.

Assuming that the total number of stress cycles $\sigma_{a,i}$ present in the process $S(t)$ is calculated as $N_{total} = \sum_{i=1}^{I} n_i$, the probability f_i that a stress amplitude, $\sigma_{a,i}$, occur will be approximated by the relation:

$$f_i = \frac{n_i}{N_{total}} \tag{39}$$

So, substituting Eq. (39) in Eq. (36), an approximation for the total fatigue damage can be written as:

$$D = \sum_{i=1}^{I} \frac{f_i N_{total}}{N_{f_i}} \tag{40}$$

By using the linear S–N model (Eq. (37) and Eq. (38)), the expression for fatigue damage is:

$$D = \frac{N_{total}}{k} \sum_{i=1}^{I} \sigma_{a_i}^m f_i \tag{41}$$

Recalling the concept of n-order statistical moment, we can express the sum of Eq. (41) as:

$$E(\sigma_{a_i}^m) = \sum_{i=1}^{I} \sigma_{a_i}^m f_i \tag{42}$$

As a result, the Eq. (41) will take the following form:

$$D = \frac{N_{total}}{k} E(\sigma_{a_i}^m) \tag{43}$$

Assume that the PSD of stress amplitude σ_a can be treated as a continuous random variable, the expected value of σ_a is:

$$E(\sigma_{a_i}^m) = \int_0^\infty \sigma_a^m f_{\sigma_a}(\sigma_a) d\sigma_a \tag{44}$$

That is, the total accumulated damage can be calculated using the following general equation:

$$D = \frac{N_{total}}{k} \int_0^\infty \sigma_a^m f_{\sigma_a}(\sigma_a) d\sigma_a \tag{45}$$

5.2.1 Fatigue damage under narrowband Gaussian loading

If the loading history is stationary narrowband Gaussian, the probability density function of the stress amplitude, $f_{\sigma_a}(\sigma_a)$, follows a Rayleigh distribution. Consequently, the total accumulated damage will be calculated using the following equation:

$$D = \frac{N_{total}}{K} E(\sigma_{a_i}^m) = \frac{N_{total}}{K} (\sqrt{2\lambda_0})^m \, \Gamma\left(\frac{m}{2} + 1\right) \tag{46}$$

where, $\Gamma(.)$ is the gamma function, and λ_0 is the variance of $S(t)$. For narrowband histories, N_{total} can be obtained as the product of the zero-crossing rate, v_0, and T is the total lifetime.

Finally, the damage caused by the history of narrowband loading and the expected life of the component can be obtained through the equations:

$$D_{NB} = \frac{v_0 T}{K} (\sqrt{2\lambda_0})^m \, \Gamma\left(\frac{m}{2} + 1\right) \tag{47}$$

$$T_{NB} = \frac{K D_{NB}}{v_0 (\sqrt{2\lambda_0})^m \, \Gamma\left(\frac{m}{2} + 1\right)} \tag{48}$$

5.2.2 Fatigue damage under broadband Gaussian loading

When the spectral characteristics of the stress history do not have characteristics of a narrow-band Gaussian process, the probability density function of the stress amplitudes, $f_{\sigma_a}(\sigma_a)$, does not follow a Rayleigh distribution.

In such situations, the function $f_{\sigma_a}(\sigma_a)$ tends to be dependent on the irregularity factor, α, as illustrated in Figure 5.3. This Figure presents 3 Gaussian histories with their respective probability density functions, $f(S(t))$ and $f_{\sigma_a}(\sigma_a)$, and spectral density function, $G(f)$. Looking at this figure, it can be noted that only the functions $f_{\sigma_a}(\sigma_a)$ and $G(f)$ vary with the irregularity factor, α. This implies that for a broadband process the relation of the peak distribution and cycle amplitudes is much more complex. For this reason, several empirical solutions have been proposed. Below we present some of the many models available in the literature.

Wirsching–Light method

Wirsching and Light [1980] used an additional spectral width parameter α_2 (see Eq. (34)) to correct the narrow-band approximation with the empirical factor ζ:

$$D_{BB} = \gamma D_{NB} \tag{49}$$

where D_{BB} is the damage accumulated due to the application of a broadband process (our wide-band process), D_{NB} is the damage accumulated is the accumulated damage calculated through Eq. (47) and ζ is the correction factor, calculated using the following equation:

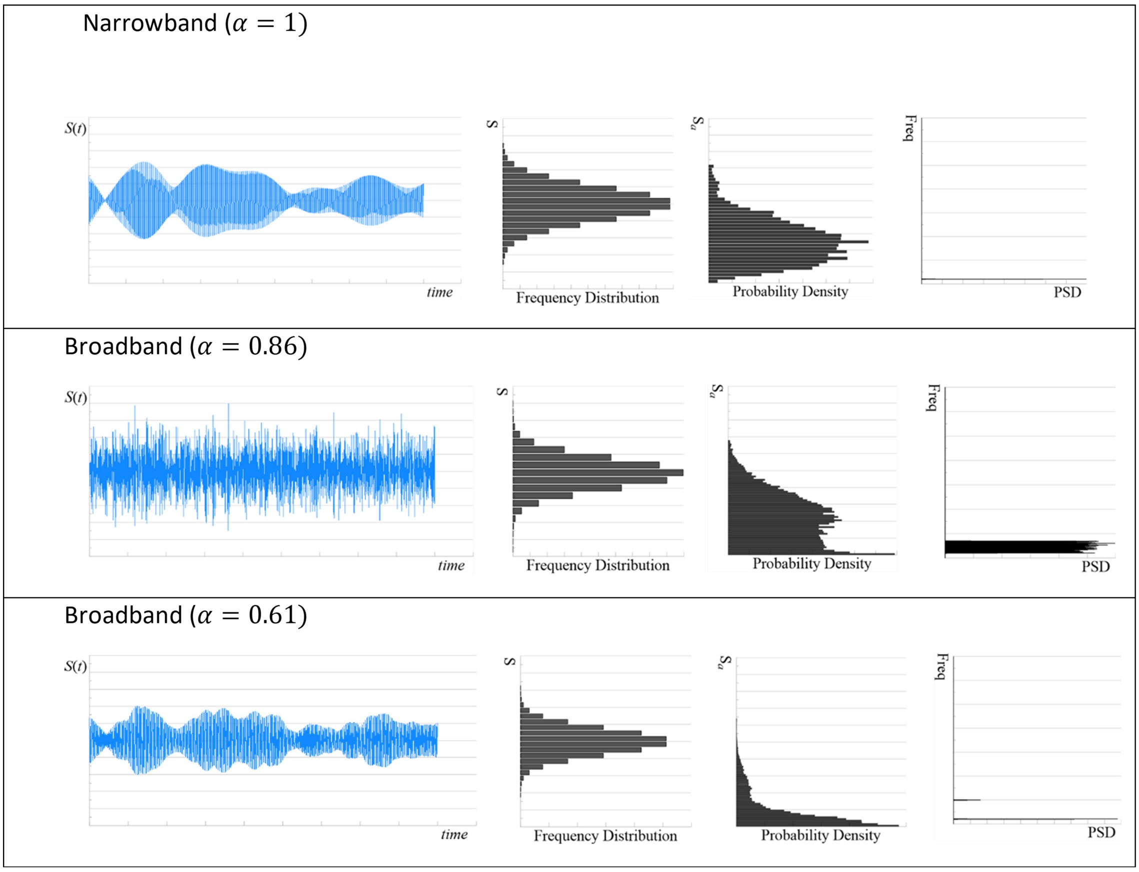

Figure 23: Characteristics of the Gaussian loading as a function of the irregularity factor.

$$\zeta = a + [1-a](1-\gamma)^b \tag{50}$$

$$a = 0,926 - 0,033k \tag{51}$$

$$b = (-1)\cdot(2.323) + 1.587k \tag{52}$$

where γ is the spectral width parameter, $\gamma = \sqrt{1-\alpha^2}$, and a (Eq. (51)) and b (Eq. (52)) are the best fitting parameters dependent on the slope of the S–N curve, k (see Eq. (19)).

Tovo–Benasciutti method

Benasciutti and Tovo [2005] first proposed an approach where the fatigue life is calculated as a linear combination of the upper and lower fatigue-damage intensity limits. The final expression for the estimated fatigue-damage intensity is:

$$D_{TB} = \eta_{NB} D_{NB} \tag{53}$$

where $\eta_{TB} = w + (1-w)\alpha_2^{(k-1)}$ considered as a narrowband damage correction factor. The weighting factor w is conditioned to the power spectrum through the parameters of the irregularity factor as follows:

$$w = \frac{(\alpha_1-\alpha_2)\left[1,112(1+\alpha_1\alpha_2-(\alpha_1+\alpha_2))e^{2,11\alpha_2}+(\alpha_1-\alpha_2)\right]}{(\alpha_2-1)^2} \tag{54}$$

The analysis of Eq. (53) indicates that, indicates that, according to the model of Tovo and Benasciutti, the damage estimate is linked to four spectral moments through parameters α_1 and α_2, showing a clear dependence of the spectral properties.

Dirlik method

Dirlik [1985] based on extensive Monte Carlo simulations of load histories, it developed a closed form empirical expression from the approximation of the probability density function of the "rainflow amplitude" as the sum of an Exponential distribution and two Rayleigh distributions. That is, the Dirlik damage model for a time period studied T is shown by the equation:

$$E[D] = D_{DK} = \frac{v_p T}{C}\int_0^\infty S_a^k f_{S_a}(S_a)dS_a \tag{55}$$

where the probability density function, $f_{S_a}(S_a)$, takes the following form:

$$f_{DK}(S_a) = \frac{1}{\sigma_s}\left(\frac{D_1}{Q}e^{\left(\frac{-Z}{Q}\right)} + Z\frac{D_2}{R^2}e^{\left(\frac{-z^2}{2R^2}\right)} + ZD_3 e^{\left(\frac{-Z^2}{2}\right)}\right) \tag{56}$$

where the function parameters are defined as:

$$Z = \frac{S_a}{\sqrt{M_0}} \tag{57}$$

$$X_m = \frac{M_1}{M_0}\sqrt{\frac{M_2}{M_4}} \tag{58}$$

$$D_1 = \frac{2(X_m-\gamma^2)}{1+\gamma^2} \tag{59}$$

$$R = \frac{\gamma - X_m - D_1^2}{1-\gamma-D_1+D_1^2} \tag{60}$$

where Z is the normalized stress amplitude (S_a) and X_m, D_1, D_2, D_3, R and Q are best-fitting parameters. Substituting these parameters in Eq. (53), the expected value of the cumulative damage over a time T is estimated by Eq. (61) - The steps necessary to obtain this formula are presented in Appendix B.

$$D_{DK} = \frac{N_{DK}}{C}\sigma_S^k \left[D_1 Q^k \Gamma(1+k) + 2^{(\frac{k}{2})}\Gamma\left(1+\frac{k}{2}\right)(D_2|R|^k + D_3)\right] \tag{61}$$

in which $N_D K$ is the total number of cycles in $S(t)$ over a period of time T ($N_{DK} = v_P T$).

Zhao and Baker method

With the objective to describe the stress range distribution, Zhao and Baker [1992] have proposed that the peak distribution function can be approximated by a linear combination between the distribution functions of Weibull and Rayleigh, with parameters directly estimated from the power spectral density function, PSD, of the process.

$$f_{ZB}(Z) = \omega\beta\lambda Z^{\beta-1}e^{-\lambda Z^\beta} + (1-\omega)Z^{\frac{Z^2}{2}} \tag{62}$$

where Z is the normalized amplitude defined above, ω is a weighting factor ($0 \leq \omega \leq 1$), and b, λ are the Weibull parameters ($b > 0, \lambda > 0$). As commented, previous parameters depended on the spectral density of process $S(t)$ and are approximated on the basis of both simulation results and theoretical arguments. Specifically, β, λ, and ω, are defined as:

$$\beta = \begin{cases} 1.1, & \text{if } \gamma \leq 0.9 \\ 1.1 + 9(\gamma - 0.9), & \text{if } \gamma > 0.9 \end{cases} \tag{63}$$

$$\lambda = 8 - 7\gamma \tag{64}$$

$$\omega = \frac{1-\gamma}{1 - \Gamma(1+\frac{1}{\beta})\lambda^{\frac{-1}{\beta}}\sqrt{\frac{2}{\pi}}} \tag{65}$$

Thereby, considering this hypothesis, a Gaussian process, $S(t)$, with average zero, the expected value of the cumulative damage over a time T is estimated by Eq. (66).

$$E[D] = D_{ZB} = \frac{N_{ZB}}{A}\sigma_s^m \left[\omega\lambda^{\frac{-m}{\beta}}\Gamma\left(1+\frac{m}{\beta}\right) + (1-\omega)2^{\frac{m}{2}}\Gamma\left(1+\frac{m}{2}\right)\right] \tag{66}$$

in which N_{ZB} is the total number of cycles in S(t) over a period of time T ($N_{ZB} = v_P T$).

Example 5.1 A hot-rolled component made of 1045 steel Q&T (BHN=410) is subjected to random loading process. The fatigue strength coefficient, S_f, and the fatigue strength exponent, b, are 3906 MPa and -0.167, respectively. The stress response at a critical location is calculated in terms of the PSD in Fig. 24. The PSD has a frequency band varying between 2 and 6 Hz with $G(f)$ = 12,500 and another one varying between 10 and 20 Hz with $G(f)$ = 5,000. Determine the fatigue life of this component using fatigue prediction models under wide-band Gaussian loading.

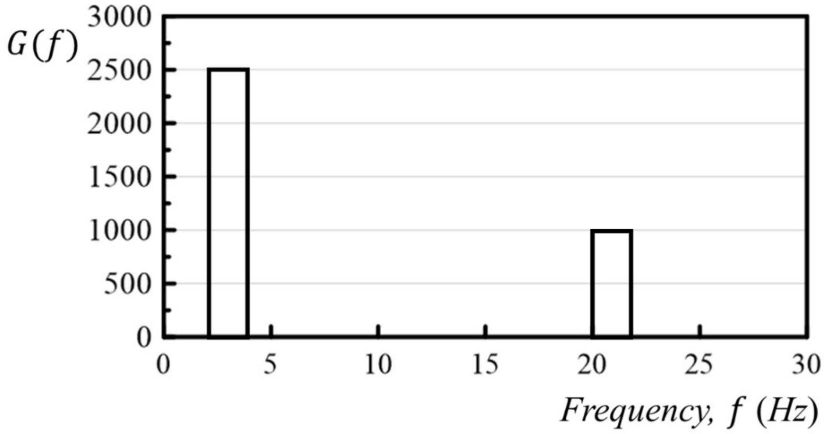

Figure 24: PSD of the stress response of a component.

Development:

We will first calculate the component fatigue damage in the frequency domain and then we will make the life estimation considering the time domain method (Rainflow) that we will use as a reference standard to compare the spectral methods.For each model we will calculate the cumulative damage per second, $\Delta_{(\ **)}$, and then calculate the total lifetime of the component, $T_{(\ **)}$.

Definition of S-N curve parameters used in spectral models:

The parameters of the S–N curve of the material presented in the test follow Eq 5.10a:

$$\sigma_{a_i} = AN_{f_i}^{-b} \tag{67}$$

Whereas the material S–N curve for vibration fatigue usually follows the following expression:

$$N_{f_i}\sigma_{a_i}^m = k \tag{68}$$

where A is the fatigue strength coefficient and b is the fatigue strength exponent. And:

$$m = \frac{1}{b} \tag{69}$$

$$k = A^m \tag{70}$$

Thus, from these considerations we will find the following values for the constants C and k:

$$k = 5,988 \tag{71}$$

$$C = 3,1216 \cdot 10^{21}\ [cycle\ \cdot\ MPa^k] \tag{72}$$

Determination of spectral moments of n-order, M_n:

The parameters used in the methods based on the frequency domain are obtained from the spectral moments extracted from the PSD of the load history acting on the component. Such moments are easily calculated using the following expressions:

$$M_0 := \int_{L1_i}^{L1_f} f^0 \cdot G_1(f)\,\mathrm{d}f + \int_{L2_i}^{L2_f} f^0 \cdot G_2(f)\,\mathrm{d}f = 7 \cdot 10^3$$

$$M_1 := \int_{L1_i}^{L1_f} f^1 \cdot G_1(f)\,\mathrm{d}f + \int_{L2_i}^{L2_f} f^1 \cdot G_2(f)\,\mathrm{d}f = 5.7 \cdot 10^4$$

$$M_2 := \int_{L1_i}^{L1_f} f^2 \cdot G_1(f)\,\mathrm{d}f + \int_{L2_i}^{L2_f} f^2 \cdot G_2(f)\,\mathrm{d}f = 9.293 \cdot 10^5$$

$$M_3 := \int_{L1_i}^{L1_f} f^3 \cdot G_1(f)\,\mathrm{d}f + \int_{L2_i}^{L2_f} f^3 \cdot G_2(f)\,\mathrm{d}f = 1.871 \cdot 10^7$$

$$M_4 := \int_{L1_i}^{L1_f} f^4 \cdot G_1(f)\,\mathrm{d}f + \int_{L2_i}^{L2_f} f^4 \cdot G_2(f)\,\mathrm{d}f = 3.912 \cdot 10^8$$

where $L1_i = 2Hz$, $L1_f = 4Hz$, $L2_i = 20Hz$, $L2_f = 22Hz$, $G_1(f) = 2,500$ and $G_2(f) = 1,000MPa^2/Hz$.

Determination of spectral Parameters:

"root mean square"	$RMS := \sqrt{M_0} = 83.666$
"zero crossing rate"	$\nu_0 := \sqrt{\frac{M_2}{M_0}} = 11.522$
"Peak occurrence rate"	$\nu_p := \sqrt{\frac{M_4}{M_2}} = 20.518$
"Irregularity Factor"	$\alpha_2 := \frac{\nu_0}{\nu_p} = 0.562$
"Spectral Width Parameter"	$\gamma := \sqrt{1 - {\alpha_2}^2} = 0.827$

Applying the Methods:

1. Narrowband Method

$$\Delta_{NB} := \frac{\nu_0}{C} \cdot (2 \cdot M_0)^{\frac{k}{2}} \cdot \Gamma\left(\frac{k}{2} + 1\right) = 5.529 \cdot 10^{-8}$$

$$\Delta_{NB} = 5.529 \cdot 10^{-8} \qquad T_{NB} := \frac{1}{\Delta_{NB} \cdot 24 \cdot 3600} = 209$$

2. Wirsching and Light Method

$$a := 0.929 - 0.033 \cdot k = 0.731$$

$$b := -2.323 + 1.587 \cdot k$$

$$\zeta := a + (1 - a) \cdot \left(1 - \gamma^2\right) = 0.816$$

$$\Delta_{WL} := \zeta \cdot \Delta_{NB} = 4.512 \cdot 10^{-8}$$

$$\Delta_{WL} = 4.512 \cdot 10^{-8} \qquad T_{WL} := \frac{1}{\Delta_{WL} \cdot 24 \cdot 3600} = 257$$

3. Tovo–Benasciutti Method

$$\alpha_1 := \frac{M_1}{\sqrt{M_0 \cdot M_2}} = 0.707 \qquad \alpha_2 := \frac{M_2}{\sqrt{M_0 \cdot M_4}} = 0.562$$

$$w := \frac{(\alpha_1 - \alpha_2) \cdot \left(\left(1.112 \cdot (1 + \alpha_1 \cdot \alpha_2 - (\alpha_1 + \alpha_2)) \right) \cdot e^{2.11 \cdot \alpha_2} + (\alpha_1 - \alpha_2) \right)}{(\alpha_2 - 1)^2} = 0.463$$

$$\eta_{TB} := w + (1 - w) \cdot {\alpha_2}^{k-1} = 0.493$$

$$\Delta_{TB} := \eta_{TB} \cdot \Delta_{NB} = 2.725 \cdot 10^{-8}$$

$$\Delta_{TB} = 2.725 \cdot 10^{-8} \qquad T_{TB} := \frac{1}{\Delta_{TB} \cdot 24 \cdot 3600} = 425$$

4. Zhao and Baker Method

$$\beta(\gamma) := \left\| \begin{array}{l} \text{if } \gamma \le 0.9 \\ \quad \| R \leftarrow 1.1 \\ \text{else} \\ \quad \| R \leftarrow 1.1 + 9 \cdot (\gamma - 0.9) \\ R \end{array} \right. = 1.1 \qquad \lambda := 8 - 7 \cdot \gamma$$

$$\omega := \frac{1 - \gamma}{1 - \Gamma\left(1 + \frac{1}{\beta(\gamma)}\right) \cdot \lambda^{-\left(\frac{1}{\beta(\gamma)}\right)} \cdot \sqrt{\frac{2}{\pi}}} = 0.558$$

$$\Delta_{ZB} := \frac{\nu_p}{C} \cdot {M_0}^{\frac{k}{2}} \cdot \left(\omega \cdot \lambda^{\frac{-k}{\beta(\gamma)}} \cdot \Gamma\left(1 + \frac{k}{\beta(\gamma)}\right) + (1 - \omega) \cdot 2^{\left(\frac{k}{2}\right)} \cdot \Gamma\left(1 + \frac{k}{2}\right) \right) = 4.361 \cdot 10^{-8}$$

$$\Delta_{ZB} = 4.361 \cdot 10^{-8} \qquad T_{ZB} := \frac{1}{\Delta_{ZB} \cdot 24 \cdot 3600} = 265$$

5. Dirlik Method

$$X_m := \frac{M_1}{M_0} \cdot \sqrt{\frac{M_2}{M_4}} = 0.397 \qquad D_1 := \frac{2 \cdot \left(X_m - \gamma^2\right)}{1 + \gamma^2} = 0.124$$

$$R := \frac{\gamma - X_m - {D_1}^2}{1 - \gamma - D_1 + {D_1}^2} = 0.453 \qquad D_2 := \frac{1 - \gamma - D_1 + {D_1}^2}{1 - R} = 0.603$$

$$D_3 := 1 - D_1 - D_2 = 0.273 \qquad Q := \frac{1.25 \cdot (\gamma - D_3 - R \cdot D_2)}{D_1} = 0.155$$

$$\Delta_{Dk} := \frac{\nu_p}{C} \cdot {M_0}^{\frac{k}{2}} \cdot \left(D_1 \cdot Q^k \cdot \Gamma(1 + k) + 2^{\frac{k}{2}} \cdot \Gamma\left(1 + \frac{k}{2}\right) \cdot \left(D_2 \cdot |R|^k + D_3\right) \right) = 2.742 \cdot 10^{-8}$$

$$\Delta_{Dk} = 2.742 \cdot 10^{-8} \qquad T_{Dk} := \frac{1}{\Delta_{Dk} \cdot 24 \cdot 3600} = 422$$

Applying the time domain method:

A basic routine for predicting fatigue life using the time domain method is presented in Appendix 1. This routine uses together the rainflow counting technique and Miner's rule. White noise filtering was used to generate the load history. As a result of using this methodology, the following results were found: Δ_{TD}=2.8649e^{-08} and T_{TD} = 404 dias.

Results Comparison:

Table 3: Table of Results Comparison.

Frequency Domain Method	$\Delta_{(**)}$	$T_{(**)}$	**Error in relation to the time domain method (%)**
NarrowBand	5.53E-08	209	-48,3
Wirsching and Light	5.51E-08	257	-36,4
Tovo–Benasciutti	2.73E-08	425	5,2
Zhao and Baker	4.36E-08	265	-34,4
Dirlik	2.74E-08	422	4,5

Comparing the results of the frequency-based life prediction models with the result obtained using the time-based life prediction model (gold standard), it is verified that the methods of Dirlik and of Tovo and Benasciutti are the methods that present results very close to those obtained by the methodology considered gold standard.

6 Introduction: Multiaxial fatigue e Maximum Variance Method (MVM)

The life prediction for mechanical components subject to the phenomenon of fatigue has evolved with new fatigue models to ensure reliability and safety in mechanical system designs. According to Papadopoulos [2001], it is of greater interest to industries to build projects that ensure high cycle fatigue strength and, consequently, a finite fatigue life around thousands or millions of loading cycles.

Multiaxial fatigue is a general term that can be used to describe a structural failure process associated with mechanical component loads and geometry that are responsible for generating complex states of stress and strain in preferred planes, which induce the initiation and propagation of cracks. Therefore, evaluating mechanical components against fatigue is a complex problem that must be handled in an appropriate manner during a mechanical design in order to avoid catastrophic failures.

There are several examples of engineering scenarios that induce the multiaxial fatigue process, such as mechanical structures subject to cyclic loads (aircraft in flight, wind regime in wind turbines, wave action in offshores, liquid flow and vibrations in industrial pipes, etc. ..) and the presence of a notch in the component geometry that can change the stress state to multiaxial.

Over the years, in order to understand the multiaxial fatigue failure mechanism, three main types of approach have been developed: Critical Plane Method, Dissipated Energy Method and Mesoscopic Deformation Models. In this chapter, the multiaxial fatigue models will be discussed, which are based on the critical plane approach and consider that the cracks, originated due to material fatigue, originate in certain material planes where the combination of normal and shear stresses or strains are extremely severe. .

Among the varieties of experimentally validated solutions for mechanical problems involving multiaxial fatigue, the Maximum Variance Method (MVM) hypothesizes that the critical plane coincides with the material plane that experiences the maximum variance of a given driving force, such as the maximum normal stress and the maximum amplitude of resolved shear stress in a given direction. This simplification allows to work with one-dimensional quantities if the problem is treated in terms of the shear stress in the direction of maximum variance $\tau_{MV}(t)$ and the stress normal $\sigma_n(t)$. Based on modern studies of variable amplitude cyclic loading, the next topics will present MVM-based multiaxial fatigue criteria:

- **MVM based on equivalent normal stress and power density function of equivalent normal stress**: consists in the analysis of load history in the time domain and spectral analysis in the frequency domain in order to compare the critical planes and obtain the equivalent normal stress and the power spectral density function equivalent, as shown in Table 4. In addition, it also has the application of the cycle counting method such as Rainflow for the time domain and, using the spectral parameters, the spectral method with correction, as Wirsching and Light [1980] for example, for the frequency domain. The driving force that induces the failure process for the time and frequency domains are respectively the equivalent normal stress and the equivalent power spectral density function, as presented in the references Łagoda et al. [2005], Nieslony and Macha [2007] and Niesłony et al. [2020].

Table 4: Approaches used by MVM based on equivalent normal stress and power density function of equivalent normal stress.

Task	Variable
Material Plane	ϕ and θ
Maximum Variance Method (MVM)	σ_{eq} and G_{eq}
Damage Accumulation	Rainflow and Palmgren-Miner Rule

- **MVM based on shear stress resolved in the direction of maximum variance**: consists of a reformulation of the Maximum Variance Method (MMV) to make it suitable in multiaxial fatigue evaluations by numerical post-processing of loading histories as complex as those that damage mechanical components real, as shown in the references Susmel and Lazzarin [2002], Susmel [2010], Susmel and Taylor [2012] and Luo et al. [2020]. The methodology presents an addition of a third orientation angle to a generic vector $\boldsymbol{q}$, following the Taylor nomenclature, and the driving force that induces fatigue failure is the shear stress, as shown in Table 5. The cycle counting method is maintained, again using the Rainflow method and Miner's Rule. The results will be compared with a time domain model and life prediction against failure proposed by Lagoda.

Table 5: Approaches used by MVM based on shear stress resolved in the direction of maximum variance.

Task	Variable
Material Plane	ϕ, θ and α
Maximum Variance Method (MVM)	τ_q
Damage Accumulation	Rainflow, Modified Wöhler Curves Method and Palmgren-Miner Rule

The advantage of MVM is that, once the variance and covariance are known, the computational time required to determine the direction that has the maximum variance of the shear stress doesn't depend strictly on the full size of the load history, but a sufficient amount of load history is required to have a stability of statistical parameters such as variance and covariance.

7 Multiaxial Fatigue - Maximum Variance Method Approach based on equivalent normal stress and power density function of equivalent normal stress

7.1 Time Domain

The stresses acting on a given plane can be deduced as long as the necessary stresses are known so that the balance of external forces belonging to the infinitesimal tetrahedron of the material body is maintained. Assuming a material point O on the inclined cutting plane as the origin of the X'-Y'-Z' coordinate system as shown in Figure 25. This point could be interpreted as the critical point in relation to fatigue strength depending on the magnitude, direction and direction of the stress vector in which it is oriented at that point. The cutting plane Δ contains perpendicularly a unit normal vector $\boldsymbol{n}$ or (n_x, n_y, n_z), being possible to determine the normal stress $\sigma_{x'}$ and the shear components $\tau_{x'y'}$ and $\tau_{x'z'}$. This plane can be referenced by its spherical coordinates θ and ϕ between 0 a 2π, however, due to the property of symmetry, the variation θ, ϕ is adopted in $[0, \pi]$ (Socie and Marquis [2000]).

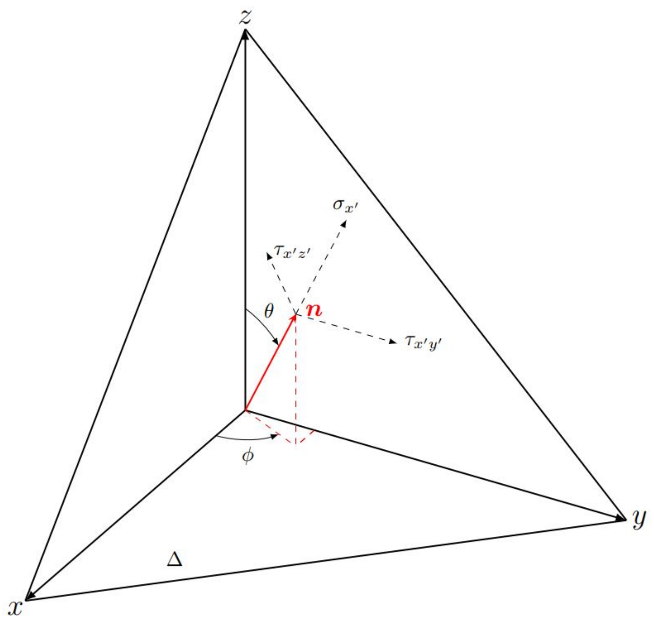

Figure 25: Stresses acting in a plane with a three-dimensional coordinate system.

Suppose a multiaxial state of stress, given by $\boldsymbol{\sigma}(t)$:

$$\boldsymbol{\sigma}(t) = \begin{bmatrix} \sigma_{xx}(t) & \tau_{xy}(t) & \tau_{xz}(t) \\ \tau_{yx}(t) & \sigma_{yy}(t) & \tau_{yz}(t) \\ \tau_{zx}(t) & \tau_{zy}(t) & \sigma_{zz}(t) \end{bmatrix} \tag{73}$$

To represent the normal stress $\sigma_{x'}$, the director cosines in function of θ and ϕ that are given according to the relations below:

$$a_{11} = \cos(\phi)\sin(\theta) \tag{74}$$
$$a_{12} = \sin(\phi)\sin(\theta) \tag{75}$$
$$a_{13} = \cos(\theta) \tag{76}$$

$$a_{21} = -\sin(\phi) \tag{77}$$
$$a_{22} = \cos(\phi) \tag{78}$$
$$a_{23} = 0 \tag{79}$$

$$a_{31} = -\cos(\phi)\cos(\theta) \tag{80}$$
$$a_{32} = -\sin(\phi)\cos(\theta) \tag{81}$$
$$a_{33} = \sin(\theta) \tag{82}$$

While, the normal vector can be given by Eq. (83):

$$\boldsymbol{n} = a_{11}\boldsymbol{i} + a_{12}\boldsymbol{j} + a_{13}\boldsymbol{k} \tag{83}$$

Therefore, the transformation equation for normal stress in any plane is given by:

$$\sigma_{x'} = \sigma_x a_{11}^2 + \sigma_y a_{12}^2 + \sigma_z a_{13}^2 + 2\left(\tau_{xy} a_{11} a_{12} + \tau_{xz} a_{11} a_{13} + \tau_{yz} a_{13} a_{12}\right) \tag{84}$$

where a_{11} , a_{12} and a_{13} are the cosines of the angles between the axes x and x', x and y' and x and z', respectively.

The Eq. (84) can be rewritten as a linear combination of the stress tensor multiplied by director cosines in the direction normal to the plane, given by Eqs. (74) to (76). Rearranging the terms:

$$\sigma_{x'} = \boldsymbol{\sigma} \cdot \boldsymbol{a} \tag{85}$$

where $\boldsymbol{\sigma}$ is the stochastic process stress vector and $\boldsymbol{a}$ is the vector of the direction cosines:

$$\mathbf{a} = \left[a_{11}^2 \ , \ a_{12}^2 \ , \ a_{13}^2 \ , \ 2a_{11}a_{12} \ , \ 2a_{11}a_{13} \ , \ 2a_{13}a_{12}\right] \tag{86}$$

$$\boldsymbol{\sigma}(t) = \left[\sigma_{xx}(t), \sigma_{yy}(t), \sigma_{zz}(t), \tau_{xy}(t), \tau_{xz}(t), \tau_{yz}(t)\right] \tag{87}$$

Applying the maximum normal stress criterion in the critical plane, it is stated that fatigue failure is caused by the maximum normal stress acting on the critical plane and that the critical plane is perpendicular to the mean direction of the maximum principal stress σ_1, according to the bibliographic reference Macha [1989]. In this way, the critical plane is defined by the direction of the normal vector $\boldsymbol{n}$, which coincides with the direction of the maximum principal stress σ_1, and, with the application of the MMV, the identification of the critical plane will be the material plane in which the variance of the equivalent stress reaches its maximum value.

Based on the normal stress transformation equation in any plane, Eq. (85) can be rewritten as a linear combination of the components of the vector **a**, represented by a_k in the crefeq:top7vector_a and modified with the directions of the normal vector **n**:

$$\sigma_{eq}(t) = \sum_{k=1}^{6} a_k \sigma_k(t) \quad (k = 1, .., 6) \tag{88}$$

With the application of the maximum normal stress criterion, the Maximum Variance Method (MVM) allows determining the plane in which the equivalent stress variance reaches its maximum value, and this plane will be considered as a critical plane and will be subject to fatigue failure:

$$var[\sigma_{eq}(t)] = \max\left(\sum_i \sum_j a_i a_j Cov\left[\sigma_i(t), \sigma_j(t)\right]\right) = \max\left(\sum_i \sum_j a_i a_j [C]\right) \tag{89}$$

where:

$$[C] = \begin{pmatrix} C_{xx,xx} & C_{xx,yy} & C_{xx,zz} & C_{xx,xy} & C_{xx,xz} & C_{xx,yz} \\ C_{yy,xx} & C_{yy,yy} & C_{yy,zz} & C_{yy,xy} & C_{yy,xz} & C_{yy,yz} \\ C_{zz,xx} & C_{zz,yy} & C_{zz,zz} & C_{zz,xy} & C_{zz,xz} & C_{zz,yz} \\ C_{xy,xx} & C_{xy,yy} & C_{xy,zz} & C_{xy,xy} & C_{xy,xz} & C_{xy,yz} \\ C_{xz,xx} & C_{xz,yy} & C_{xz,zz} & C_{xz,xy} & C_{xz,xz} & C_{xz,yz} \\ C_{yz,xx} & C_{yz,yy} & C_{yz,zz} & C_{yz,xy} & C_{yz,xz} & C_{yz,yz} \end{pmatrix} \tag{90}$$

where the covariance of two equal components of the tension tensor vector, in other words, with the same subindex ($m = n$), is equal to the variance of the component itself. Therefore, the covariance matrix can be redefined as follows:

$$[C] = \begin{pmatrix} V_{xx} & C_{xx,yy} & C_{x,zz} & C_{xx,xy} & C_{xx,xz} & C_{xx,yz} \\ C_{yy,xx} & V_{yy} & C_{yy,zz} & C_{yy,xy} & C_{yy,xz} & C_{yy,yz} \\ C_{zz,xx} & C_{zz,yy} & V_{zz} & C_{zz,xy} & C_{zz,xz} & C_{zz,yz} \\ C_{xy,xx} & C_{xy,yy} & C_{xy,zz} & V_{xy} & C_{xy,xz} & C_{xy,yz} \\ C_{xz,xx} & C_{xz,yy} & C_{xz,zz} & C_{xz,xy} & V_{xz} & C_{xz,yz} \\ C_{yz,xx} & C_{yz,yy} & C_{yz,zz} & C_{yz,xy} & C_{yz,xz} & V_{yz} \end{pmatrix} \tag{91}$$

Critical angles are determined from the critical plane, where the variance of $\sigma_{eq}(t)$ has reached its maximum value as seen in Eq. (92).

$$\theta^c, \phi^c = max[var_{\sigma_{eq}}(\theta, \phi)] \tag{92}$$

7.2 Frequency Domain

In the frequency domain, from spectral methods, there is application of spectral power density functions (PSD) to evaluate the characteristics of frequencies in the history of stress. In this way, the multiaxial stress states are described by the power spectral density function matrix $\boldsymbol{G}(f)$:

$$\boldsymbol{G}(f) = \begin{bmatrix} G_{11}(f) & G_{12}(f) & G_{13}(f) & G_{14}(f) & G_{15}(f) & G_{16}(f) \\ G_{21}(f) & G_{22}(f) & G_{23}(f) & G_{24}(f) & G_{25}(f) & G_{26}(f) \\ G_{31}(f) & G_{32}(f) & G_{33}(f) & G_{34}(f) & G_{35}(f) & G_{36}(f) \\ G_{41}(f) & G_{42}(f) & G_{43}(f) & G_{44}(f) & G_{45}(f) & G_{46}(f) \\ G_{51}(f) & G_{52}(f) & G_{53}(f) & G_{54}(f) & G_{55}(f) & G_{56}(f) \\ G_{61}(t) & G_{62}(f) & G_{63}(f) & G_{64}(f) & G_{65}(f) & G_{66}(f) \end{bmatrix} \tag{93}$$

As shown in the bibliographic reference Nieslony and Macha [2007], from the power spectral density matrix $\boldsymbol{G}(f)$, $G_{eq}(f)$ can be obtained by Eq. (94):

$$G_{eq}(f) = \boldsymbol{a}\boldsymbol{G}(f)\boldsymbol{a}^{\boldsymbol{T}} \tag{94}$$

Solving the inner product, Eq. (94) will be represented as follows:

$$G_{eq} = a_1^2 G_{11} + a_1 a_4 G_{41} + a_1 a_4 G_{14} + a_4^2 G_{44} = a_1^2 G_{11} + a_4^2 G_{44} + (a_1 a_4)(G_{41} + G_{14}) \tag{95}$$

$$G_{eq} = a_1^2 G_{11} + a_4^2 G_{44} + 2 a_1 a_4 \mathfrak{Re}(G_{41}) \tag{96}$$

The application of the MMV in the frequency domain occurs in a similar way to the time domain, with identification of the maximum value of variance of power density function of equivalent normal stress, proposed in Eq. (97), in which the vector of the coefficients coincides with the $\boldsymbol{a}$ vector of the linear combination:

$$var[G_{eq}(f)] = \sum_i \sum_j a_i a_j var(G_{kl}) \tag{97}$$

$$var(G_{kl}) = \mathfrak{Re}\left[\int_0^\infty G_{kl}(f) df\right] \quad \text{(k,l=1,...,6)} \tag{98}$$

The power spectral density matrix is given by real parts of zero-order spectral moments of power spectral density functions. By MMV method, identifying the critical angles where the variance has its maximum value:

$$\theta^c, \phi^c = max[var_{G_{eq}}(\theta, \phi)] \tag{99}$$

It is worth mentioning that the variance obtained is also the spectral moment of the equivalent power spectral density function as shown by Eq. (100):

$$var(G_{eq}) = m_{o,G_{eq}} = \mathfrak{Re}\left[\int_0^\infty G_{eq}(f)df\right] \tag{100}$$

Therefore, the number of oscillations, also known as crossover rate, and the number of local peaks are given respectively by Eq. (101) and Eq. (102). While the number of oscillations and local peaks of the equivalent spectral density function is given by Eq. (103) and Eq. (104).

$$N_o^+ = \sqrt{\frac{m_2}{m_0}} \tag{101}$$

$$M^+ = \sqrt{\frac{m_4}{m_2}} \tag{102}$$

$$N_o^+ = \sqrt{\frac{m_{2,G_{eq}}}{m_{0,G_{eq}}}} \tag{103}$$

$$M^+ = \sqrt{\frac{m_{4,G_{eq}}}{m_{2,G_{eq}}}} \tag{104}$$

8 Multiaxial Fatigue - Maximum Variance Method Approach based on shear stress resolved in the direction of maximum variance

To formalize the theory, we consider a body in a frame of reference O_{xyz} subjected to a complex system of forces and moments that result in a three-dimensional state of stress that varies over time. The generic material plane, as shown in Fig. 26, can be oriented by the angles θ and ϕ through a normal vector $\boldsymbol{n}$, while the second frame of reference $O_{e_a e_b n}$, a local coordinate system belonging to a generic material plane where the normal vector passes through the point of origin, has its orientation defined by other unit vectors $\boldsymbol{e_a}$ and $\boldsymbol{e_b}$ whose cross product of these vectors results in the normal vector, as shown in Fig. 26. Using the critical plane method, it is possible to identify the orientation of a generic plane in the form of the previous coordinate system, xyz.

According to Figure Fig. 26, Fig. 27 and Fig. 28, the unit vectors that define the orientation of the axes $\boldsymbol{n}$, $\boldsymbol{e_a}$ e $\boldsymbol{e_b}$ [3] plane can be expressed as follows:

$$\boldsymbol{n} = \begin{bmatrix} n_x \\ n_y \\ n_z \end{bmatrix} = \begin{bmatrix} \sin\theta\cos\phi \\ \sin\theta\sin\phi \\ \cos\theta \end{bmatrix} \tag{105}$$

$$\boldsymbol{e_a} = \begin{bmatrix} e_{a_x} \\ e_{a_y} \\ e_{a_z} \end{bmatrix} = \begin{bmatrix} \sin\phi \\ -\cos\phi \\ 0 \end{bmatrix} \tag{106}$$

$$\boldsymbol{e_b} = \begin{bmatrix} e_{b_x} \\ e_{b_y} \\ e_{b_z} \end{bmatrix} = \begin{bmatrix} \cos\theta\cos\phi \\ \cos\theta\sin\phi \\ -\sin\theta \end{bmatrix} \tag{107}$$

[3] $\boldsymbol{e_b}$: to project this unit vector it is necessary to project in the plane zb_θ for later decompose it into the xy.

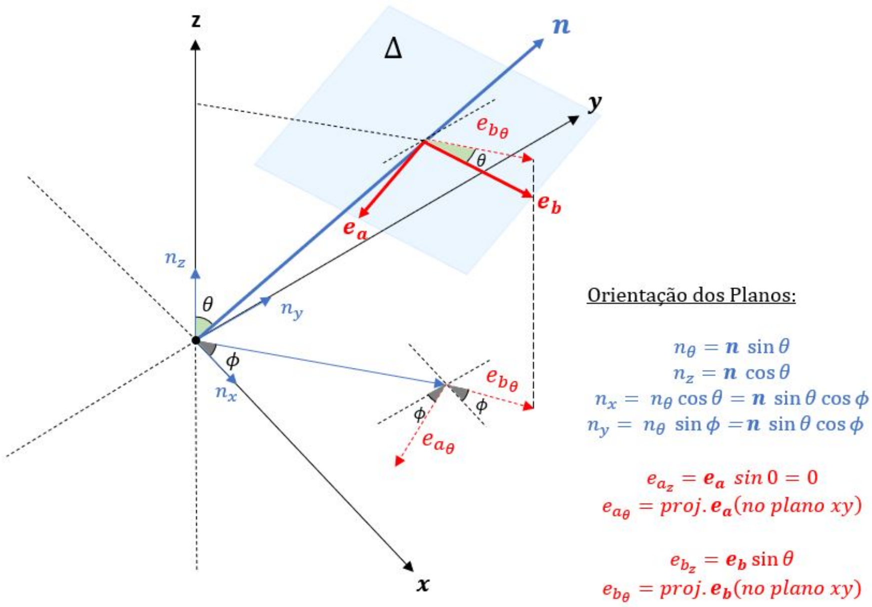

Figure 26: Stresses acting in a plane with a three-dimensional coordinate system (Courtesy of Lima [2021])

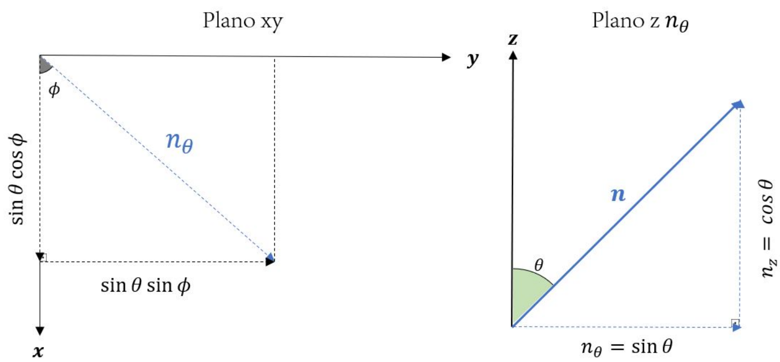

Figure 27: Projection of unit vector n (Courtesy of Lima [2021]).

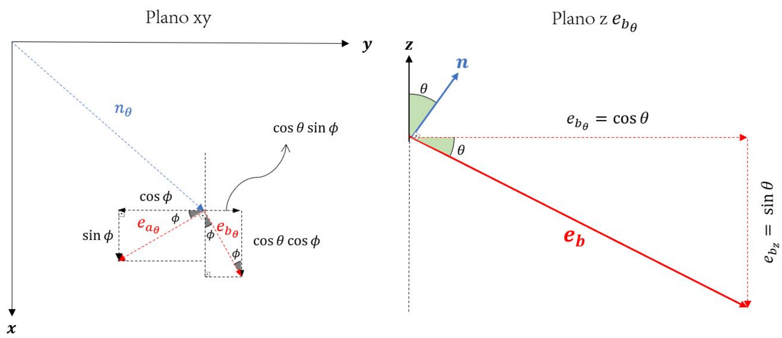

Figure 28: Projection of unit vector e_a and e_b (Courtesy of Lima [2021]).

Based on Fig. 28, Susmel assumed a generic direction m for the unit vector $\boldsymbol{q}$ in a given material plane situated in the new coordinate system and oriented by the angle α between unit vector $\boldsymbol{a}$ and unit vector $\boldsymbol{q}$. As Fig. 29, the components of $\boldsymbol{q}$ vector can be written in the following vector form:

$$\boldsymbol{q} = \boldsymbol{q}_{\boldsymbol{e_a}} + \boldsymbol{q}_{\boldsymbol{e_b}} \tag{108}$$

$$\boldsymbol{q} = \boldsymbol{e_a} \cos\alpha + \boldsymbol{e_b} \sin\alpha \tag{109}$$

$$\boldsymbol{q} = \begin{bmatrix} \cos\alpha\sin\phi + \sin\alpha\cos\theta\cos\phi \\ -\cos\alpha\cos\phi + \sin\alpha\cos\theta\sin\phi \\ -\sin\alpha\sin\theta \end{bmatrix} \tag{110}$$

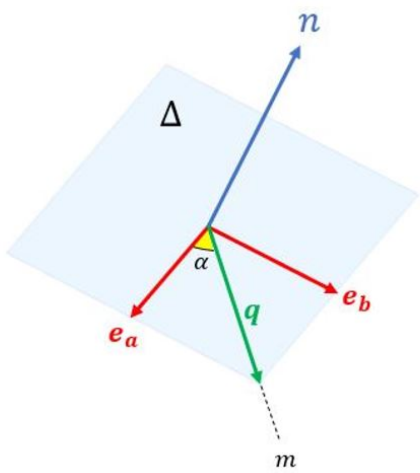

Figure 29: Projection of vector $\boldsymbol{q}$ in vector e_a and e_b (Courtesy of Lima [2021]).

$$\sigma_n(t) = \begin{bmatrix} n_x & n_y & n_z \end{bmatrix} \begin{bmatrix} \sigma_{xx}(t) & \tau_{xy}(t) & \tau_{xz}(t) \\ \tau_{yx}(t) & \sigma_{yy}(t) & \tau_{yz}(t) \\ \tau_{zx}(t) & \tau_{zy}(t) & \sigma_{zz}(t) \end{bmatrix} \begin{bmatrix} n_x \\ n_y \\ n_z \end{bmatrix} \tag{111}$$

$$\tau_q(t) = \begin{bmatrix} q_x & q_y & q_z \end{bmatrix} \begin{bmatrix} \sigma_{xx}(t) & \tau_{xy}(t) & \tau_{xz}(t) \\ \tau_{yx}(t) & \sigma_{yy}(t) & \tau_{yz}(t) \\ \tau_{zx}(t) & \tau_{zy}(t) & \sigma_{zz}(t) \end{bmatrix} \begin{bmatrix} n_x \\ n_y \\ n_z \end{bmatrix} \tag{112}$$

Developing Eq. (112), the instantaneous value of the resolved shear stress along the m direction:

$$\tau_q(t) = \boldsymbol{q}^T\, \overline{\sigma}(t)\, \boldsymbol{n} \tag{113}$$

$$\begin{aligned}\tau_q(t) = n_x \cdot (q_z \cdot \tau_{xz} + q_y \cdot \tau_{xy} + q_x \cdot \sigma_{xx}) + n_y \cdot (q_z \cdot \tau_{yz} + q_x \cdot \tau_{xy} + q_y \cdot \sigma_{yy}) \\ + n_z \cdot (q_y \cdot \tau_{yz} + q_x \cdot \tau_{xz} + q_z \cdot \sigma_{zz})\end{aligned} \tag{114}$$

Rearranging Eq. (114), isolating the stress terms:

$$\begin{aligned}\tau_q(t) = \sigma_x \cdot (n_x \cdot q_x) + \sigma_{yy} \cdot (n_y \cdot q_y) + \sigma_{zz} \cdot (n_z \cdot q_{zz}) + \tau_{xy} \cdot (n_x \cdot q_y + n_y \cdot q_x) \\ + \tau_{xz} \cdot (n_x \cdot q_z + n_z \cdot q_x) + \tau_{yz} \cdot (n_y \cdot q_z + n_z \cdot q_y)\end{aligned} \tag{115}$$

Rewriting tensor in Voigt's Notation, the representation of $\boldsymbol{\sigma}(t)$ would be a six-dimensional vector process and, therefore, the shear stress can be expressed as:

$$\tau_q(t) = \boldsymbol{d} \cdot \boldsymbol{s}(t) \tag{116}$$

Where the tensor in Voigt notation is given as follows:

$$\boldsymbol{s}(t) = \boldsymbol{\sigma}^T(t) = \begin{bmatrix} \sigma_{xx}(t) & \sigma_{yy}(t) & \sigma_{zz}(t) & \tau_{xy}(t) & \sigma_{xz}(t) & \sigma_{yz}(t) \end{bmatrix} \tag{117}$$

Where $\boldsymbol{d}$ is known as the vector of director cosines, being expressed according to Eq. (118):

$$\boldsymbol{d} = \begin{bmatrix} d_1 \\ d_2 \\ d_3 \\ d_4 \\ d_5 \\ d_6 \end{bmatrix} = \begin{bmatrix} n_x \cdot q_x \\ n_y \cdot q_y \\ n_z \cdot q_z \\ n_x \cdot q_y + n_y\, q_x \\ n_x \cdot q_z + n_z\, q_x \\ n_y \cdot q_z + n_z\, q_y \end{bmatrix} = \begin{bmatrix} \frac{1}{2}\left[\sin(\theta)\sin(2\phi)\cos(\alpha) + \sin(\alpha)\sin(2\theta)\cos(\phi)^2\right] \\ \frac{1}{2}\left[-\sin(\theta)\sin(2\phi)\cos(\alpha) + \sin(\alpha)\sin(2\theta)\sin(\phi)^2\right] \\ -\frac{1}{2}\sin(\alpha)\sin(2\theta) \\ \frac{1}{2}\sin(\alpha)\sin(2\phi)\sin(2\theta) - \cos(\alpha)\cos(2\phi)\sin(\theta) \\ \sin(\alpha)\cos(\phi)\cos(2\theta) + \cos(\alpha)\sin(\phi)\cos(\theta) \\ \sin(\alpha)\sin(\phi)\cos(2\theta) - \cos(\alpha)\cos(\phi)\cos(\theta) \end{bmatrix} \tag{118}$$

The model formulation is based on the assumption that fatigue damage maximizes in a plane that experiences the maximum amplitude of shear stress. From shear stress of a generic direction m, τ_q, the MVM identifies the critical plane from the variance of the resolved shear stress history in the direction in which it reaches its maximum value. With this, the variance of shear stress, $\tau_q(t)$, resolved along the direction m can then be calculated directly as:

$$var[\tau_q(t)] = \boldsymbol{d}^T [C] \boldsymbol{d} \tag{119}$$

$$var[\tau_q(t)] = \begin{bmatrix} d_1 & d_2 & d_3 & d_4 & d_5 & d_6 \end{bmatrix} \begin{bmatrix} C_{xx,xx} & C_{xx,yy} & C_{xx,zz} & C_{xx,xy} & C_{xx,xz} & C_{xx,yz} \\ C_{yy,xx} & C_{yy,yy} & C_{yy,zz} & C_{yy,xy} & C_{yy,xz} & C_{yy,yz} \\ C_{zz,xx} & C_{zz,yy} & C_{zz,zz} & C_{zz,xy} & C_{zz,xz} & C_{zz,yz} \\ C_{xy,xx} & C_{xy,yy} & C_{xy,zz} & C_{xy,xy} & C_{xy,xz} & C_{xy,yz} \\ C_{xz,xx} & C_{xz,yy} & C_{xz,zz} & C_{xz,xy} & C_{xz,xz} & C_{xz,yz} \\ C_{yz,xx} & C_{yz,yy} & C_{yz,zz} & C_{yz,xy} & C_{yz,xz} & C_{yz,yz} \end{bmatrix} \begin{bmatrix} d_1 \\ d_2 \\ d_3 \\ d_4 \\ d_5 \\ d_6 \end{bmatrix} \tag{120}$$

Or by Taylor series expansion as:

$$var[\tau_q(t)] = var\left[\sum_k d_k \sigma_k\right] = \sum_i \sum_j d_i d_j Cov\left[\sigma_i, \sigma_j\right] \tag{121}$$

Another way to simplify of Eq. (119) would be to consider the product of the covariance matrix and the vector $\boldsymbol{d}$ as a column matrix $[M]$.

$$[M] = \begin{bmatrix} M_1 \\ M_2 \\ M_3 \\ M_4 \\ M_5 \\ M_6 \end{bmatrix} = \begin{bmatrix} C_{xx,xx} & C_{xx,yy} & C_{xx,zz} & C_{xx,xy} & C_{xx,xz} & C_{xx,yz} \\ C_{yy,xx} & C_{yy,yy} & C_{yy,zz} & C_{yy,xy} & C_{yy,xz} & C_{yy,yz} \\ C_{zz,xx} & C_{zz,yy} & C_{zz,zz} & C_{zz,xy} & C_{zz,xz} & C_{zz,yz} \\ C_{xy,xx} & C_{xy,yy} & C_{xy,zz} & C_{xy,xy} & C_{xy,xz} & C_{xy,yz} \\ C_{xz,xx} & C_{xz,yy} & C_{xz,zz} & C_{xz,xy} & C_{xz,xz} & C_{xz,yz} \\ C_{yz,xx} & C_{yz,yy} & C_{yz,zz} & C_{yz,xy} & C_{yz,xz} & C_{yz,yz} \end{bmatrix} \begin{bmatrix} d_1 \\ d_2 \\ d_3 \\ d_4 \\ d_5 \\ d_6 \end{bmatrix} \tag{122}$$

And in the form of Taylor series expansion, the variance can be expressed as:

$$var[\tau_q(t)] = \sum_{i=1}^{6} d_i M_i \tag{123}$$

In this way, the variance of shear stress in the direction of vector ***q*** of Eq. (119) can be represented as follows:

$$var[\tau_q(t)] = \begin{bmatrix} d_1 & d_2 & d_3 & d_4 & d_5 & d_6 \end{bmatrix} \begin{bmatrix} M_1 \\ M_2 \\ M_3 \\ M_4 \\ M_5 \\ M_6 \end{bmatrix} \tag{124}$$

Critical angles are determined from the critical plane, where the variance of $\tau_q(t)$ has reached its maximum value as seen in Eq. (125).

$$\theta^c, \phi^c, \alpha^c = max[var_{\tau_q}(\theta, \phi, \alpha)] \tag{125}$$

9 Multiaxial Fatigue - Maximum Variance Method Approach as a function of the invariants of deviatoric stress tensor: Projection-by-Projection (PbP)

Among the stress invariant-based methods to estimate fatigue life, the approach called "Projection by Projection – Projection-by-Projection (PbP)" is suitable for multiaxial fatigue analysis. The proposed criterion is particularly useful for the evaluation of the durability of complex structures under random loading. The advantages of the PbP method can be obtained in the time domain, as well as for applications in the frequency domain (Benasciutti et al. [2013])

In 2008, the first works published with the PbP method were developed by Cristofori, Susmel and Tovo (Cristofori et al. [2008]), who described the time domain methodology to estimate fatigue damage in the presence of complex multiaxial loads. In 2011, Cristofori, Benasciutti and Tovo (Cristofori et al. [2011]) continued the development of the method and published the formulation for the frequency domain, which can be applied to stationary multiaxial random loads. In 2014, a numerical example for analyzing a steel beam excited by a random input acceleration was proposed by Cristofori and Benasciutti (Cristofori and Benasciutti [2014]), who performed a finite element analysis to calculate the PSD stress matrix at the nodes of the structure and applied the spectral model of the PbP method to estimate the fatigue damage. A practical guide for implementing the method in the frequency domain was presented by Benasciutti, Zanellati and Cristofori in 2019 (Benasciutti et al. [2019]), which detailed all the steps of the method. These are the most relevant works developed so far for the PbP method, which include numerical examples and/or procedures for implementing the method.

9.1 Projection-by-Projection (PbP)

This method makes use of the amplitude of the second invariant of the deviator tensor $\sqrt{(J_{2a})}$ and the hydrostatic pressure $\sigma_H(t)$ to evaluate the damage due to a generic fatigue loading. The fatigue life of a real component is estimated considering the loading history described in 5-dimensional Euclidean space, in which the damage related to a generic loading path can be determined from the contributions calculated by the projection of the loading trajectory itself to the along the axes of a chosen frame of reference based on Euclidean space (Cristofori et al. [2008]).

From a geometric point of view, the loading trajectory can be fully represented in terms of its projections along the directions of maximum variance defined by the axes of the chosen frame of reference and adopted based on the 5-dimensional deviator space. In this way, analysis of a complex loading trajectory can be performed from its projections, such that the damage relative to each projection can be calculated first, and then the overall damage from the loading history can be obtained as a function of the different contributions given by the projections (Cristofori et al. [2008]).

The procedure adopted by the PbP method to estimate fatigue life consists of defining the reference of the projection system, evaluating the damage along each projection and, finally, evaluating the total damage.

In this sense, considering that $\boldsymbol{\sigma}(t)$ represents the tensor of the time-varying stress components

$$\boldsymbol{\sigma}(t) = \begin{bmatrix} \sigma_{xx}(t) & \tau_{xy}(t) & \tau_{xz}(t) \\ \tau_{xy}(t) & \sigma_{yy}(t) & \tau_{yz}(t) \\ \tau_{xz}(t) & \tau_{yz}(t) & \sigma_{zz}(t) \end{bmatrix} \quad \longrightarrow \quad \boldsymbol{\sigma}(t) = \begin{bmatrix} \sigma_{xx}(t) \\ \sigma_{yy}(t) \\ \sigma_{zz}(t) \\ \tau_{xy}(t) \\ \sigma_{xz}(t) \\ \sigma_{yz}(t) \end{bmatrix} \tag{126}$$

The six non-redundant stress components of the $\boldsymbol{\sigma}(t)$ can be reordered into a stress vector which, in the frequency domain, can be characterized by the PSD matrix, $\boldsymbol{G}(f)$

$$\boldsymbol{G}(f) = \begin{bmatrix} G_{11}(f) & G_{12}(f) & G_{13}(f) & G_{14}(f) & G_{15}(f) & G_{16}(f) \\ G_{21}(f) & G_{22}(f) & G_{23}(f) & G_{24}(f) & G_{25}(f) & G_{26}(f) \\ G_{31}(f) & G_{32}(f) & G_{33}(f) & G_{34}(f) & G_{35}(f) & G_{36}(f) \\ G_{41}(f) & G_{42}(f) & G_{43}(f) & G_{44}(f) & G_{45}(f) & G_{46}(f) \\ G_{51}(f) & G_{52}(f) & G_{53}(f) & G_{54}(f) & G_{55}(f) & G_{56}(f) \\ G_{61}(t) & G_{62}(f) & G_{63}(f) & G_{64}(f) & G_{65}(f) & G_{66}(f) \end{bmatrix} \tag{127}$$

where $\boldsymbol{G}(f)$ is the matrix of autospectral and cross-spectral density functions of stress vector $\boldsymbol{\sigma}(t)$.

The set of zero-order spectral moments of the PSD matrix ($\boldsymbol{G}(f)$) is represented in the covariance matrix:

$$Var(G_{kl}) = \mathfrak{Re}\left[\int_0^\infty G_{kl}(f)df\right] \quad \text{(k,l=1,...,6)} \tag{128}$$

$$\boldsymbol{C} = \begin{bmatrix} V_x & C_{xx,yy} & C_{xx,zz} & C_{xx,xy} & C_{xx,xz} & C_{xx,yz} \\ C_{yy,xx} & V_y & C_{yy,zz} & C_{yy,xy} & C_{yy,xz} & C_{yy,yz} \\ C_{zz,xx} & C_{zz,yy} & V_z & C_{zz,xy} & C_{zz,xz} & C_{zz,yz} \\ C_{xy,xx} & C_{xy,yy} & C_{xy,zz} & V_{xy} & C_{xy,xz} & C_{xy,yz} \\ C_{xz,xx} & C_{xz,yy} & C_{xz,zz} & C_{xz,xy} & V_{xz} & C_{xz,yz} \\ C_{yz,xx} & C_{yz,yy} & C_{yz,zz} & C_{yz,xy} & C_{yz,xz} & V_{yz} \end{bmatrix} \tag{129}$$

where the diagonal elements are the variance terms of the stress $x_i(t), C_{ii} = Var(x_i(t))$, and the off-diagonal elements are the covariance terms between the stress $x_i(t)$ and $x_j(t)$, $C_{ij} = Cov(x_i(t), x_j(t))$. The coefficient of correlation $r_{ij}, r_{ij} = C_{ij}/\sqrt{(C_{ii}C_{jj})}$, represents, for multiaxial random loads, the degree of proportionality between $x_i(t)$ and $x_j(t)$. When $r_{ij} = 1$, the processes are perfectly correlated, that is, proportional stresses, when $r_{ij} = 0$, they are uncorrelated processes, that is, non-proportional stresses (Cristofori et al. [2011], Benasciutti et al. [2019])

Fatigue damage from a multiaxial random stress is addressed by the PbP method in the deflector space. Thus, the vector of stresses in the deviator space, $\boldsymbol{s}(t)$, is related to the stress tensor $\boldsymbol{\sigma}(t)$ by the following transformation rules:

$$\boldsymbol{s}(t) = \begin{bmatrix} s_1(t) \\ s_2(t) \\ s_3(t) \\ s_4(t) \\ s_5(t) \end{bmatrix} \tag{130}$$

where:

$$s_1(t) = \frac{1}{2\sqrt{3}}(2\sigma_{xx}(t) - \sigma_{yy}(t) - \sigma_{zz}(t)) \tag{131}$$

$$s_2(t) = \frac{1}{2}(\sigma_{yy}(t) - \sigma_{zz}(t)) \tag{132}$$

$$s_3(t) = \tau_{xy}(t) \tag{133}$$

$$s_4(t) = \tau_{zx}(t) \tag{134}$$

$$s_5(t) = \tau_{yz}(t) \tag{135}$$

The stochastic vector $\boldsymbol{s}(t)$ that describes the stress components in the deviator space can be characterized by the covariance matrix C' and in the frequency domain by the PSD 5x5 matrix $\boldsymbol{G'}(f)$ (Cristofori and Benasciutti [2014]). The axes of the projections are defined in the direction of maximum variance of the deviator space, so from the eigenvectors $\boldsymbol{U}$ of the covariance matrix $\boldsymbol{C'}$ the projections of the stress histories in time are described as:

$$\boldsymbol{\Omega}(t) = \boldsymbol{U}^T\boldsymbol{s}(t) \quad \text{where} \quad \boldsymbol{\Omega}(t) = (\Omega_{(p,1)}(t), \Omega_{(p,2)}(t), \Omega_{(p,3)}(t), \Omega_{(p,4)}(t), \Omega_{(p,5)}(t)) \tag{136}$$

$$\boldsymbol{C'_p}(t) = \boldsymbol{U}^T\boldsymbol{C'}(t)\boldsymbol{U} \tag{137}$$

where $\boldsymbol{\Omega}(t)$ represents the projections in the direction of maximum variance and $\boldsymbol{C'_p}(t)$ is a diagonal matrix of variance of the vector $\Omega(t)$:

$$C'_{p,ii} = Var[\Omega_{(p,i)}] \quad i = 1, 2, \ldots, 5. \tag{138}$$

In the frequency domain, the diagonal PSD matrix $\boldsymbol{G'_p}(f)$ determines the power spectra in the projections:

$$\boldsymbol{G'_p}(f) = \boldsymbol{U}^T\boldsymbol{G'}(t)\boldsymbol{U} \tag{139}$$

Therefore, the projections of random stresses $\Omega_(p,i)(t)$ of the vector $\boldsymbol{\Omega}(t)$ are totally uncorrelated, where each component represents an independent random stress, and its fatigue damage can be estimated separately either in the time domain and frequency (Cristofori and Benasciutti [2014]).

9.2 PbP Method for a Plane Stress State

In the plane or biaxial stress state, the stress tensor becomes three non-redundant stress components:

$$\boldsymbol{\sigma}(t) = \begin{bmatrix} \sigma_{xx}(t) & \tau_{xy}(t) \\ \tau_{xy}(t) & \sigma_{yy}(t) \end{bmatrix} = \begin{bmatrix} \sigma_{xx}(t) \\ \sigma_{yy}(t) \\ \tau_{xy}(t) \end{bmatrix} \tag{140}$$

where $\boldsymbol{\sigma}(t)$ can be represented as stress vector, where each stress is considered a stationary random variable Benasciutti et al. [2019]. In the frequency domain, the PSD matrix is now represented as:

$$\boldsymbol{G}(f) = \begin{bmatrix} G_{11}(f) & G_{12}(f) & G_{13}(f) \\ G_{21}(f) & G_{22}(f) & G_{23}(f) \\ G_{31}(f) & G_{32}(f) & G_{33}(f) \end{bmatrix} = \begin{bmatrix} G_{xx}(f) & G_{xx,yy}(f) & G_{xx,xy}(f) \\ G_{yy,xx}(f) & G_{yy}(f) & G_{yy,xy}(f) \\ G_{xy,xx}(f) & G_{xy,yy}(f) & G_{xy}(f) \end{bmatrix} \tag{141}$$

Consequently, the covariance matrix will take the form:

$$\boldsymbol{C} = \begin{bmatrix} C_{xx} & C_{xx,yy} & C_{xx,zz} \\ C_{yy,xx} & C_{yy} & C_{yy,zz} \\ C_{xy,xx} & C_{xy,yy} & C_{xy} \end{bmatrix} = \begin{bmatrix} V_{xx} & C_{xx,yy} & C_{xx,zz} \\ C_{yy,xx} & V_{yy} & C_{yy,zz} \\ C_{xy,xx} & C_{xy,yy} & V_{xy} \end{bmatrix} \tag{142}$$

The stress vector in the deviator space becomes three dimensional, $\boldsymbol{s}(t) = [s_1(t), s_2(t), s_3(t)]$, which can be determined as:

$$\boldsymbol{s}(t) = \boldsymbol{A} \cdot \boldsymbol{x}(t) \tag{143}$$

where:

$$\boldsymbol{A} = \begin{bmatrix} \frac{1}{\sqrt{3}} & -\frac{1}{2\sqrt{3}} & 0 \\ 0 & \frac{1}{2} & 0 \\ 0 & 0 & 1 \end{bmatrix} \tag{144}$$

The covariance matrix and the PSD of $\boldsymbol{s}(t)$ can be obtained from the matrix $\boldsymbol{A}$ through the following equations:

$$\boldsymbol{C'} = \boldsymbol{A} \cdot \boldsymbol{C} \cdot \boldsymbol{A^T} = \begin{bmatrix} C'_{11} & C'_{12} & C'_{13} \\ & C'_{22} & C'_{23} \\ sim & & C'_{33} \end{bmatrix} \tag{145}$$

$$\boldsymbol{G'}(f) = \boldsymbol{A} \cdot \boldsymbol{G}(f) \cdot \boldsymbol{A^T} \tag{146}$$

Thus, from the eigenvectors $\boldsymbol{U}$ of the covariance matrix $\boldsymbol{C'}$, the loadings in the projections with the direction of maximum variance are obtained:

$$\boldsymbol{\Omega}(t) = \boldsymbol{U}^T \boldsymbol{s}(t) \quad \text{where} \quad \boldsymbol{\Omega}(t) = [\Omega_{(p,1)}(t), \Omega_{(p,2)}(t), \Omega_{(p,3)}(t)] \tag{147}$$

The covariance matrix of the vector $\boldsymbol{\Omega}(t)$ is determined as:

$$\boldsymbol{C'_p} = \boldsymbol{U^T} \cdot \boldsymbol{C'} \cdot \boldsymbol{U} = \begin{bmatrix} C'_{p,11} & 0 & 0 \\ 0 & C'_{p,22} & 0 \\ 0 & 0 & C'_{p,33} \end{bmatrix} \tag{148}$$

and in the frequency domain the PSD matrix is defined:

$$\boldsymbol{G'_p}(f) = \boldsymbol{U}^T \boldsymbol{G'}(t) \boldsymbol{U} = \begin{bmatrix} G'_{p,11}(f) & 0 & 0 \\ 0 & G'_{p,22}(f) & 0 \\ 0 & 0 & G'_{p,33}(f) \end{bmatrix} \tag{149}$$

The principle of the PbP method can be illustrated through Fig. 30, in which a random loading history of bending and torsion $[\sigma_{xx}(t), \tau_{xy}(t)]$ is represented in the deviator space with two non-zero components $[s_1(t), s_3(t)]$ that generate a random loading path Ψ. To define the reference of the projection system $[s_1, 0, s_3, 0]$ the direction of maximum variance of the loading Ψ is considered, thus obtaining the projections of stress $[\Omega_{(p,1)}(t), \Omega_{(p,3)}(t)]$.

For fatigue life estimation under multiaxial conditions, the Modified Wöhler Curve Method (MWCM) proposed by Susmel and Lazzarin [2002]. The MWCM takes as its starting point the assumption that crack initiation is Mode II dominated, and it holds true independently of both stress concentration feature and degree of multiaxiality of the stress field damaging the fatigue process zone (Susmel and Taylor [2003], Susmel [2004]). In more detail, the MWCM assumes that fatigue damage depends on the shear stress amplitude, τ_a, and on the maximum normal stress, $\sigma_{(n,max)}$, relative to the critical plane, which is defined as the plane experiencing the maximum shear stress amplitude. From a practical point of view, the MWCM postulates that fatigue damage depends on two stress parameters: τ_a and ρ . The latter parameter is defined as the ratio between the maximum normal stress, $\sigma_{(n,max)}$, and the shear stress amplitude, τ_a, relative to the critical plane (Araújo et al. [2007]).

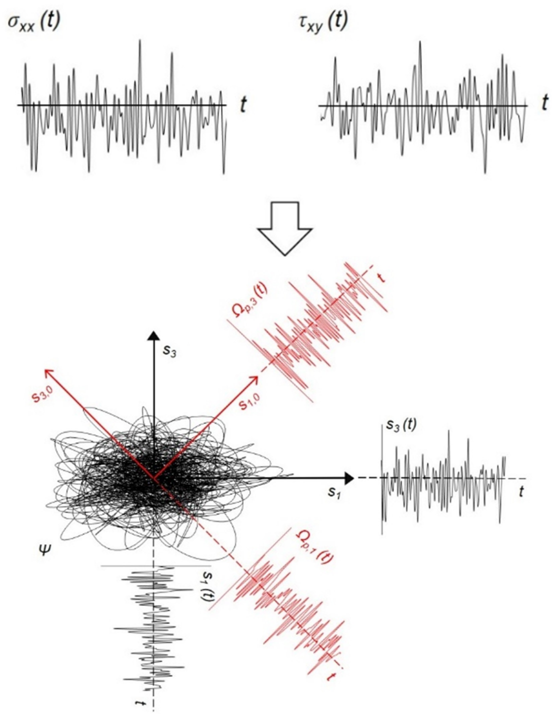

Figure 30: Example of a random loading path Ψ in the deflector space, generated from flexural-torsional stresses, to determine the stresses in the reference frame of the projection system

The modified Wöhler diagram used to define the parameters of the S-N curve in multiaxial loading situations considers two fatigue curves that are generally available for materials: a normal stress versus life curve obtained under fully reverse loading conditions, characterized by $\rho = 1$ (just normal stree and see Fig. 31), and a fatigue curve obtained under fully reverse torsional conditions, characterized by $\rho = 0$ (just shear stress and see Fig. 31).

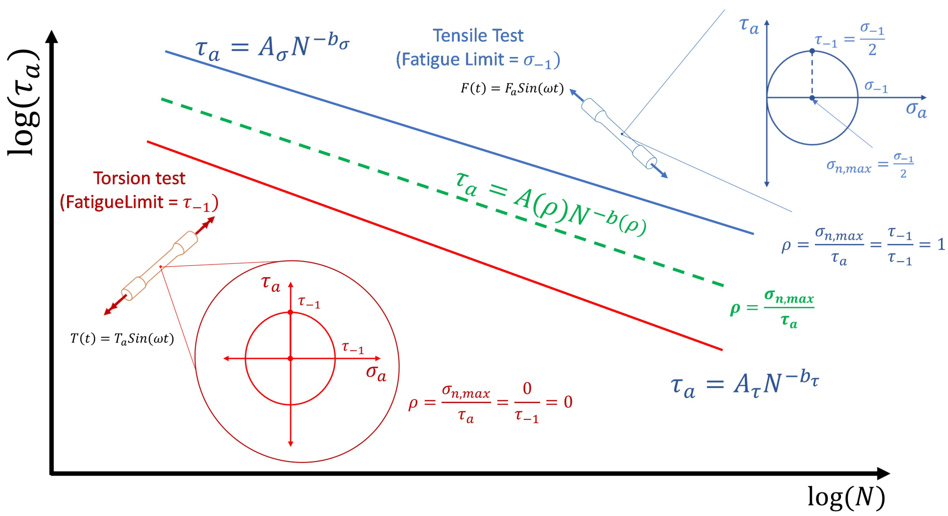

Figure 31: Modified Wöhler diagram for defining the reference S-N curve for a generic multiaxial loading.

Hypothetically, it is assumed that the reference S-N curve in the modified Wöhler diagram for any given value of ρ is defined by linear interpolation of the fatigue parameters for axial and torsional loading (Benasciutti et al. [2019]). From the definition of the multiaxiality degree in the critical plane (ρ_{crit}), the parameters that characterize the curve τ_a versus N_f respectively, $A_{\rho_{crit}}$ (coefficient of the τ_a-N curve) and $b_{\rho_{crit}}$ (curve exponent), can be estimated by means of Eq. (150) and Eq. (151).

$$A_{\rho_{crit}} = [A_\sigma - A_\tau]\rho_{crit} + A_\tau \tag{150}$$

$$b_{\rho_{crit}} = [b_\sigma - b_\tau]\rho_{crit} + b_\tau \tag{151}$$

9.3 Life Prediction Strategies Using the PbP Method

Life prediction by the PbP method can be performed in both time and frequency domains, the main difference between the two domains being the determination of the S-N reference curve in the modified Wöhler diagram. Once the ρ_ref parameter is defined, according to each domain, the parameters of the S-N curve are defined by Equation (9.17) and then the damage estimate is performed, which in time considers the rainflow technique associated with the Palmgren-Miner rule and follows the development presented in Section 4, for the frequency domain, it analyzes the power spectra as shown in Section 5.

9.3.1 Application of the Life Estimation in the Time Domain

The rainflow counting method can be applied to each projection of the loading history in the U_i directions, where the amplitude of the cycles defined in terms of the deviator stress $J_{a_{ij}}$, and the values of the maximum hydrostatic pressure $\sigma_{H_{ij}}$, are recorded for each cycle. counted (identified by the subscript j) along each considered projection (identified by the subscript $i = 1, 2, \cdots, 5$) (Cristofori et al. [2008]). In order to estimate fatigue damage, the reference curve in the modified Wöhler diagram can be located from the stress ratio ρ_{ref} defined as:

$$\rho_{ref} = \sqrt{3}\frac{\sigma_{(H_{ref})}}{\left(\sum_i (J_{a_{iref}})^2\right)^{1/2}} \tag{152}$$

where $J_{a_{iref}}$ is the average value of the amplitude for the cycles counted in relation to the considered projection and $\sigma_{H_{ref}}$ the average value of the maximum hydrostatic stresses of the cycles, defined by the following relations:

$$\sigma_{H_{ref}} = mean_{ij}[\sigma_{(H_{ij})}] \tag{153}$$

$$J_{a_{iref}} = mean_{ij}[J_{(a_{ij})}] \tag{154}$$

where $\sigma_H = trace(\boldsymbol{\sigma})/3$ is the hydrostatic stress.

The fatigue damage, D_{ij}, due to each identified cycle can then be estimated using the following equation:

$$D_{ij} = \left[\frac{J_{a_{ij}}}{J_{a,ref}}\right]^{k_{ref}} \frac{1}{N_A} \tag{155}$$

and the total damage relative to the i-th projection D_i, considering the linear cumulative rule proposed by Palmgren-Miner, results in the estimation of the damage $D(\Omega_{p,i})$ related to the projected loading $\Omega_{p,i}$:

$$D(\Omega_{p,i}) = \sum_j D_{ij} \tag{156}$$

Considering that the damage caused by the histories of multiaxial loads acting in the directions of the deflector tensor is decoupled, Cristofori et al. [2008] proposed the following quadratic rule to calculate the accumulated damage at the analyzed point:

$$D(\Omega) = \left[\sum_i \left(D\left(\Omega_{p,i}\right)\right)^{\frac{2}{k_{ref}}}\right] = \left[\sum_i \left(\sum_j D_{ij}\right)^{\frac{2}{k_{ref}}}\right]^{\frac{k_{ref}}{2}} \tag{157}$$

9.3.2 Application of the Life Estimation in the Frequency Domain

To take full advantage of a frequency domain approach, the definition of the stress ratio ρ_{ref} must be properly reformulated for stationary multiaxial random loading. This is accomplished by considering the following equation:

$$\rho_{ref} = \sqrt{3}\frac{\frac{\sigma_{H,m}}{\sqrt{2}} + \sqrt{Var(\sigma_H(t))}}{\sqrt{\sum_i Var(\Omega_{p,i}(t))}} = \sqrt{3}\frac{\sigma_{H,m} + \sqrt{2\lambda_{0,H}}}{\sqrt{2\sum_i \lambda_{0,i}}} \tag{158}$$

where $\sigma_H(t)$ is the hydrostatic stress, a uniaxial stationary random process, with constant mean $\sigma_{H,m}$ and variance $Var(\sigma_H(t)) = \lambda_{0,H}$ (which coincides with the zero-order moment $\lambda_{(0,H)}$ of the power spectral density $G_H(f)$ of $\sigma_H(t)$). Likewise, every projection $\Omega_{p,i}(t)$ is a stationary random process, with variance $Var(\Omega_{(p,i)}(t)) = \lambda_{0,i}$ (where $\lambda_{0,i}$ is the zero-order moment of the power spectral density $G'_{p,i}(f)$ of the loading history in each of the "i" projections, which is an element of the matrix $G'_p(f)$) (Cristofori et al. [2011]). If the multiaxial loading has stress components with an average value of zero, then $\sigma_{H,m} = 0$. In the case of sinusoidal loading of constant amplitude, Eq. (158) reduces to the expression of Eq. (152).

In the frequency domain an estimate of the expected damage in a time interval can be provided by spectral methods. If the random projection $\Omega_{p,i}(t)$ is a narrow band process the damage is defined as:

$$D_{NB}(\Omega_{p,i}) = \frac{v_{0,i}T}{C_{ref}}(\sqrt{2\lambda_{0,i}})^{k_{ref}}\Gamma\left(1 + \frac{k_{ref}}{2}\right) \tag{159}$$

and the total damage of the multiaxial loading histories is defined from the quadratic accumulation rule:

$$D_{NB}^{PbP} = \frac{T}{C_{ref}}\Gamma\left(1 + \frac{k_{ref}}{2}\right)\left[\sum_i \left(2\lambda_{0,i}(v_{o,i})^{\frac{2}{k_{ref}}}\right)\right]^{\frac{k_{ref}}{2}} \tag{160}$$

If the random projection $\Omega_{p,i}(t)$ is a broadband process, the damage can be estimated by other spectral methods, such as the Tovo-Benasciutti method (cited in Section 5.2.2).

$$D_{TB}(\Omega_{p,i}) = \eta_{TB,i}\frac{v_{o,i}T}{C_{ref}}(\sqrt{2\lambda_{0,i}})^{k_{ref}}\Gamma\left(1 + \frac{k_{ref}}{2}\right) \tag{161}$$

so that the total damage is obtained from the consideration of all projections

$$D_{TB}^{PbP} = \frac{T}{C_{ref}}\Gamma\left(1 + \frac{k_{ref}}{2}\right)\left[\sum_i \left(2\lambda_{0,i}(\eta_{TB,i}v_{o,i})^{\frac{2}{k_{ref}}}\right)\right]^{\frac{k_{ref}}{2}} \tag{162}$$

Moreover, the theory of the PbP method can be easily extended to other spectral methods, such as Dirlik's method ((cited in section 5.2.2).). For this method the damage can be obtained as:

$$D_{DK}(\Omega_{p,i}) = \frac{v_{p,i}T\sigma_{S,i}^{k_{ref}}}{C_{ref}}\left[D_{1,i}Q_i^{k_{ref}}\Gamma(k_{ref}+1) + (\sqrt{2})^{k_{ref}}\Gamma\left(\frac{k_{ref}}{2}+1\right)(D_{2,i}|R_i|^{k_{ref}} + D_{3,i})\right] \tag{163}$$

where the total damage of the loading story consists of:

$$D_{DK}^{PbP}=\frac{T}{C_{ref}}\left[\sum_i\left(v_{p,i}^{\frac{2}{k_{ref}}}\,\sigma_{S,i}^2\left[D_{1,i}Q_i^{k_{ref}}\Gamma(k_{ref}+1)+(\sqrt{2})^{k_{ref}}\Gamma\left(\frac{k_{ref}}{2}+1\right)(D_{2,i}|R_i|^{k_{ref}}+D_{3,i})\right]\right)\right]^{\frac{k_{ref}}{2}} \tag{164}$$

10 Final Remarks

This chapter sought to present a review of the state of art and the concepts necessary to understand the criteria of multiaxial random fatigue using the Maximum Variance Method (MVM) in medium and high cycle fatigue regimes. In this sense, approaches based on time domain and frequency domain were examined. We tried, as far as possible, to structure the material presented in a amicable way and with easy-to-understand language so that it can contribute, especially for researchers who wish to start studies on this topic.

Despite the theoretical review on the phenomenology of random fatigue under uniaxial and multiaxial loading conditions and the deductions presented in the methodologies involved in this chapter, we must emphasize that all the topics discussed are in continuous development and improvement - An example is the contribution recently published in the article Ferreira et al. [2022] which presents an innovative and highly efficient strategy for the search for the critical plane based on the maximum variance of resolved shear stress method. Comparative tests showed that the proposed algorithm is, on average, 150 times faster than the search strategy based on the Gradient Ascent Method and at least 230 times faster than the Direct Search Method of critical planes.

References

J. Araújo, L. Susmel, D. Taylor, J. Ferro, and E. Mamiya. On the use of the theory of critical distances and the modified wöhler curve method to estimate fretting fatigue strength of cylindrical contacts. *International Journal of Fatigue*, 29(1):95–107, 2007. ISSN 0142-1123. doi: https://doi.org/10.1016/j.ijfatigue.2006.02.041.

ASTM-E1049-85. Standard practices for cycle counting in fatigue analysis. Technical report, ASTM International, West Conshohocken, PA, 2017.

D. Benasciutti and R. Tovo. Spectral methods for lifetime prediction under wide-band stationary random processes. *International Journal of Fatigue*, 27:867–877, 08 2005. doi: 10.1016/j.ijfatigue.2004.10.007.

D. Benasciutti, A. Cristofori, and R. Tovo. Analogies between spectral methods and multiaxial criteria in fatigue damage evaluation. *Probabilistic Engineering Mechanics*, 31:39–45, 2013. ISSN 0266-8920. doi: https://doi.org/10.1016/j.probengmech.2012.12.002.

D. Benasciutti, D. Zanellati, and A. Cristofori. The "projection-by-projection" (pbp) criterion for multiaxial random fatigue loadings: Guidelines to practical implementation. *Frattura ed Integrità Strutturale*, 47:348–366, 01 2019. doi: 10.3221/IGF-ESIS.47.26.

N. Bishop. The use of frequency domain parameters to predict structural fatigue. *Tese, Department of Engineering, University of Warwick, England*, 01 1988.

A. Cristofori and D. Benasciutti. “projection-by-projection” approach: A spectral method for multiaxial random fatigue. *SAE Technical Paper 2014-01-0924*, 1, 04 2014. doi: 10.4271/2014-01-0924.

A. Cristofori, L. Susmel, and R. Tovo. A stress invariant based criterion to estimate fatigue damage under multiaxial loading. *International Journal of Fatigue*, 30(9):1646–1658, 2008. ISSN 0142-1123. doi: 10.1016/j.ijfatigue.2007.11.006.

A. Cristofori, D. Benasciutti, and R. Tovo. A stress invariant based spectral method to estimate fatigue life under multiaxial random loading. *International Journal of Fatigue*, 33:887–899, 07 2011. doi: 10.1016/j.ijfatigue.2011.01.013.

T. Dirlik. Application of computers in fatigue analysis. *Ph.D. thesis.The University of Warwick*, 1985.

T. Dirlik and D. Benasciutti. Dirlik and tovo-benasciutti spectral methods in vibration fatigue: A review with a historical perspective. *Multidisciplinary Digital Publishing Institute 11*, 11:1333, 08 2021. doi: 10.3390/met11091333.

E739-10. Standard practice for statistical analysis of linear or linearized stress-life (s-n) and strain-life (e-n) fatigue data. Technical report, ASTM International, West Conshohocken, PA, 2015.

J. Ferreira, J. Dias, E. Cardoso, J. Araújo, and C. da Silva. A contribution to the identification of the critical plane using the maximum variance method. *International Journal of Fatigue*, page 107228, 2022. ISSN 0142-1123. doi: https://doi.org/10.1016/j.ijfatigue.2022.107228.

Y.-L. Lee. Fatigue analysis in the frequency domain. *Fatigue Testing and Analysis: Theory and Practice, Yung-Li Lee, J. Pan, R. B. Hathaway e M. E. Barkey (Ed.). Elsevier Inc.*, pages 369–394, 12 2005. doi: 10.1016/B978-075067719-6/50011-7.

F. M. d. Lima. Fadiga multiaxial: Análise de espectro para previsão de vida em componentes sujeitos a carregamentos de amplitude variável. In *Projeto de Graduação (Engenharia Mecânica), Departamento de Engenharia Mecânica, Universidade de Brasília, Brasília, DF,*, page 127 p., 2021.

P. Luo, W. Yao, and L. Susmel. An improved critical-plane method and cycle counting method to assess damage under variable amplitude multiaxial fatigue loading. *Fatigue and Fracture of Engineering Materials and Structures*, 43:2024–2039, 05 2020. doi: 10.1111/ffe.13281.

E. Macha. Generalization of fatigue criteria for multiaxial sinusoidal loadings in the range of random loadings. *Biaxial and Multiaxial Fatigue*, EGF 3:425–36, 1989.

M. Matsuichi and T. Endo. Fatigue of metals subjected to varying stress. *Paper presented to Japan Soc. Mech. Engrs ,Jukvoka, Japan*, 1968.

A. Nieslony and E. Macha. *Spectral Method in Multiaxial Random Fatigue*. Lecture Notes in Applied and Computational Mechanics. Springer Berlin Heidelberg, 2007.

A. Niesłony, M. Böhm, and R. Owsiński. Formulation of multiaxial fatigue failure criteria for spectral method. *International Journal of Fatigue*, 135:105519, 06 2020. doi: 10.1016/j.ijfatigue.2020.105519.

I. Papadopoulos. Long life fatigue under multiaxial loading. *International Journal of Fatigue - INT J FATIGUE*, 23:839–849, 2001.

D. Socie and G. Marquis. *Multiaxial fatigue*. Premiere Series Bks. Society of Automotive Engineers, 2000.

L. Susmel. A unifying approach to estimate the high-cycle fatigue strength of notched components subjected to both uniaxial and multiaxial cyclic loadings. *Fatigue & Fracture of Engineering Materials & Structures*, 27:391 – 411, 04 2004. doi: 10.1111/j.1460-2695.2004.00759.x.

L. Susmel. A simple and efficient numerical algorithm to determine the orientation of the critical plane in multiaxial fatigue problems. *International Journal of Fatigue*, 32:1875–1883, 11 2010.

L. Susmel and P. Lazzarin. A bi-parametric wöhler curve for high cycle multiaxial fatigue assessment. *Fatigue & Fracture of Engineering Materials & Structures*, 25:63 – 78, 01 2002. doi: 10.1046/j.1460-2695.2002.00462.x.

L. Susmel and D. Taylor. Two methods for predicting the multiaxial fatigue limits of sharp notches. *Fatigue & Fracture of Engineering Materials & Structures*, 26:821 – 833, 09 2003. doi: 10.1046/j.1460-2695.2003.00683.x.

L. Susmel and D. Taylor. A critical distance/plane method to estimate finite life of notched components under variable amplitude uniaxial/multiaxial fatigue loading. *International Journal of Fatigue*, 38:7–24, 2012.

P. H. Wirsching and M. C. Light. Fatigue under wide band random stresses. *Journal of the Structural Division*, 106:1593–1607, 1980.

W. Zhao and M. J. Baker. On the probability density function of rainflow stress range for stationary gaussian processes. *International Journal of Fatigue*, 14:121–135, 1992.

T. Łagoda, E. MACHA, and A. Niesłony. Fatigue life calculation by means of the cycle counting and spectral methods under multiaxial random loading. *Fatigue, Fracture of Engineering Materials and Structures*, 28:409 – 420, 2005.

APPENDIX A
DEDUCTION OF THE DIRLIK DAMAGE EQUATION

The expected total fatigue damage by Dirlik's method, D_{DK}

$$D_{DK} = \frac{\nu_p\, T}{K} \int_0^{\infty} S_a^m\, P_{rr}(S_r)\, dS_r \,. \tag{A1}$$

where $P_{rr}\,(S_r)$ is the probability density function of rainflow intervals in terms of the auxiliary variable Z defined as

$$P_{rr}(S_r) = \frac{D_1}{2\sigma_S\, Q} e^{-\frac{Z}{Q}} + \frac{D_2\, Z}{2\sigma_S\, R^2} e^{-\frac{Z^2}{2R^2}} + \frac{D_3\, Z}{2\sigma_S} e^{-\frac{Z^2}{2}} \,, \tag{A2}$$

where $Z = \frac{S_r}{2\sigma_S} = \frac{S_a}{\sigma_S}$.

Therefore, we have the integral to be solved

$$I = \int_0^{\infty} S_a^m\, P_{rr}(S_r)\, dS_r = \int_0^{\infty} \left(\frac{S_r}{2}\right)^m \left[\frac{D_1}{2\sigma_S\, Q} e^{-\frac{S_r}{2\sigma_S\, Q}} + \frac{D_2\, S_r}{4\sigma_S^2\, R^2} e^{-\frac{S_r^2}{8\sigma_S^2 R^2}} + \frac{D_3\, S_r}{4\sigma_S^2} e^{-\frac{S_r^2}{8\sigma_S^2}}\right] dS_r \,. \tag{A3}$$

Separating the integral into parts

$$I = \int_0^{\infty} \left(\frac{S_r}{2}\right)^m \frac{D_1}{2\sigma_S\, Q} e^{-\frac{S_r}{2\sigma_S\, Q}}\, dS_r + \int_0^{\infty} \left(\frac{S_r}{2}\right)^m \frac{D_2\, S_r}{4\sigma_S^2\, R^2} e^{-\frac{S_r^2}{8\sigma_S^2 R^2}}\, dS_r + \int_0^{\infty} \left(\frac{S_r}{2}\right)^m \frac{D_3\, S_r}{4\sigma_S^2} e^{-\frac{S_r^2}{8\sigma_S^2}}\, dS_r \,, \tag{A4}$$

so that

$$I_1 = \int_0^{\infty} \left(\frac{S_r}{2}\right)^m \frac{D_1}{2\sigma_S\, Q} e^{-\frac{S_r}{2\sigma_S\, Q}}\, dS_r; \quad I_2 = \int_0^{\infty} \left(\frac{S_r}{2}\right)^m \frac{D_2\, S_r}{4\sigma_S^2\, R^2} e^{-\frac{S_r^2}{8\sigma_S^2 R^2}}\, dS_r;$$
$$I_3 = \int_0^{\infty} \left(\frac{S_r}{2}\right)^m \frac{D_3\, S_r}{4\sigma_S^2} e^{-\frac{S_r^2}{8\sigma_S^2}}\, dS_r \,, \tag{A5}$$

that is,

$$I = I_1 + I_2 + I_3 \,. \tag{A6}$$

Solving the integral I_1

$$I_1 = \frac{D_1}{2\sigma_S\, Q} \int_0^\infty \left(\frac{S_r}{2}\right)^m e^{-\frac{S_r}{2\sigma_S\, Q}}\, dS_r\,. \tag{A7}$$

Performing a change of variable

$$m = a - 1;\ \ \frac{S_r}{2\sigma_S\, Q} = x \ \ \text{e}\ \ dS_r = 2\sigma_S\, Q\, dx\,. \tag{A8}$$

The integral I_1 can be rewritten as

$$I_1 = \frac{D_1}{2\sigma_S\, Q} \int_0^\infty (\sigma_S\, Q\, x)^{a-1}\, e^{-x}\, 2\sigma_S\, Q\, dx = D_1\, (\sigma_S\, Q)^{a-1} \int_0^\infty x^{a-1}\, e^{-x}\, dx\,. \tag{A9}$$

Given that the gamma function is defined as

$$\Gamma(a) = \int_0^\infty x^{a-1}\, e^{-x}\, dx\,, \tag{A10}$$

the integral I_1 can be expressed based on the gamma function

$$I_1 = D_1\, (\sigma_S\, Q)^{a-1}\, \Gamma(a)\,. \tag{A11}$$

Returning from the variable change

$$I_1 = D_1\, (\sigma_S\, Q)^m \Gamma(m+1)\,. \tag{A12}$$

The integral I_2 has the following form

$$I_2 = \frac{D_2}{2\sigma_S^2\, R^2} \int_0^\infty \left(\frac{S_r}{2}\right)^{m+1} e^{-\frac{S_r^2}{8\sigma_S^2 R^2}}\, dS_r\,. \tag{A13}$$

Again, performing a change of variable

$$m + 1 = a - 1;\ \ \frac{S_r^2}{8\sigma_S^2 R^2} = x \ \ \text{e}\ \ dS_r = \frac{\sqrt{2}\, \sigma_S\, R}{\sqrt{x}}\, dx\,. \tag{A14}$$

which allows you to write it as

$$I_2 = \frac{D_2}{2\sigma_S^2\, R^2} \int_0^\infty (\sqrt{2}\sigma_S\, R\, \sqrt{x})^{a-1}\, e^{-x}\, \frac{\sqrt{2}\, \sigma_S\, R}{\sqrt{x}}\, dx = \frac{D_2}{2\sigma_S\, R}\, \sqrt{2}(\sqrt{2}\sigma_S\, R)^{a-1} \int_0^\infty (\sqrt{x})^{a-1}\, e^{-x}\, \frac{1}{\sqrt{x}}\, dx\,. \tag{A15}$$

Simplifying the expression

$$I_2 = D_2\ (2)^{\frac{a}{2}-1}(\sigma_S\ R)^{a-2}\int_0^{\infty}(\sqrt{x})^{a-2}\ e^{-x}\ dx\ . \tag{A16}$$

Performing another variable change

$$a = 2b\ , \tag{A17}$$

The I_2 can be write as

$$I_2 = D_2\ (2)^{b-1}(\sigma_S\ R)^{2b-2}\int_0^{\infty}(\sqrt{x})^{2b-2}\ e^{-x}\ dx = \ D_2\ (2)^{b-1}(\sigma_S\ R)^{2b-2}\int_0^{\infty}x^{b-1}\ e^{-x}\ dx\ . \tag{A18}$$

Using the gamma function shown in Equation (A10)

$$I_2 = D_2\ (2)^{b-1}(\sigma_S\ R)^{2b-2}\ \Gamma(b)\ . \tag{A19}$$

Returning from the variable change

$$I_2 = D_2\ (2)^{\frac{a}{2}-1}(\sigma_S\ R)^{a-2}\ \Gamma\left(\frac{a}{2}\right) = D_2\ (2)^{\frac{m}{2}}(\sigma_S\ R)^{m}\ \Gamma\left(\frac{m}{2}+1\right). \tag{A20}$$

Solving the integral I_3

$$I_3 = \frac{D_3}{2\sigma_S^2}\int_0^{\infty}\left(\frac{S_r}{2}\right)^{m+1}\ e^{-\frac{S_r^2}{8\sigma_S^2}}\ dS_r\ . \tag{A21}$$

Performing a change of variable

$$m+1 = a-1;\ \ \frac{S_r^2}{8\sigma_S^2} = x\ \ \text{e}\ \ dS_r = \frac{\sqrt{2}\ \sigma_S}{\sqrt{x}}\ dx\ . \tag{A22}$$

the integral I_3 can be rewritten as

$$I_3 = \frac{D_3}{2\sigma_S^2}\int_0^{\infty}(\sqrt{2}\sigma_S\ \sqrt{x})^{a-1}\ e^{-x}\ \frac{\sqrt{2}\ \sigma_S}{\sqrt{x}}\ dx = \frac{D_3}{2\sigma_S}\ \sqrt{2}(\sqrt{2}\sigma_S)^{a-1}\int_0^{\infty}(\sqrt{x})^{a-1}\ e^{-x}\ \frac{1}{\sqrt{x}}\ dx\ . \tag{A23}$$

Simplifying the expression

$$I_3 = D_3\ (2)^{\frac{a}{2}-1}(\sigma_S)^{a-2}\int_0^{\infty}(\sqrt{x})^{a-2}\ e^{-x}\ dx\ . \tag{A24}$$

Performing another variable change

$$a = 2b\ , \tag{A25}$$

the integral I_3 can be rewritten as

$$I_3 = D_3\ (2)^{b-1}(\sigma_S)^{2b-2}\int_0^\infty(\sqrt{x})^{2b-2}\ e^{-x}\ dx = D_3\ (2)^{b-1}(\sigma_S)^{2b-2}\int_0^\infty x^{b-1}\ e^{-x}\ dx\ . \tag{A26}$$

Using the gamma function shown in Equation (A10)

$$I_3 = D_3\ (2)^{b-1}(\sigma_S)^{2b-2}\ \Gamma(b)\ . \tag{A27}$$

Returning from variable change

$$I_3 = D_3\ (2)^{\frac{a}{2}-1}(\sigma_S)^{a-2}\ \Gamma\left(\frac{a}{2}\right) = D_3\ (2)^{\frac{m}{2}}(\sigma_S)^m\ \Gamma\left(\frac{m}{2}+1\right). \tag{A28}$$

Adding all solved integrals together

$$I = D_1\ (\sigma_S\ Q)^m\Gamma(m+1) + D_2\ (2)^{\frac{m}{2}}(\sigma_S\ R)^m\ \Gamma\left(\frac{m}{2}+1\right) + D_3\ (2)^{\frac{m}{2}}(\sigma_S)^m\ \Gamma\left(\frac{m}{2}+1\right). \tag{A29}$$

Simplifying the equation

$$I = \sigma_S^m\left[D_1\ Q^m\ \Gamma(m+1) + \left(\sqrt{2}\right)^m\ \Gamma\left(\frac{m}{2}+1\right)(D_2\ |R|^m) + D_3\right]. \tag{A30}$$

Substituting the integral into Equation (A1), the Dirlik damage at a time interval T can be determined as

$$D_{DK} = \frac{\nu_p\ T}{K}\sigma_S^m\left[D_1\ Q^m\ \Gamma(m+1) + \left(\sqrt{2}\right)^m\ \Gamma\left(\frac{m}{2}+1\right)\ (D_2|R|^m + D_3)\right]. \tag{A31}$$

APPENDIX 2

MATLAB ROUTINE FOR LIFE ESTIMATION BASED ON THE TIME DOMAIN METHOD

```
clc
clear
close all

% T = SIGNAL ACQUISITION WINDOW TIME
% RMS_sigmap = RMS VALUE OF NORMAL STRESS COMPONENT
% RMS_taup = RMS VALUE OF SHEAR STRESS COMPONENT
% ro = CORRELATION COEFFICIENT BETWEEN SIGMA AND TAU STRESS HISTORIES
% BANDA = SPECTRAL BANDWIDTH OF SIGNALS SIGNAL CENTRAL FREQUENCY
% PT_PERIODO = NUMBER OF POINTS PER PERIOD
% Fmin = LOWER LIMIT OF SIGNAL FREQUENCY BAND
% Fmax = UPPER LIMIT OF SIGNAL FREQUENCY BAND
% TAMANHO = SPECTRUM SIZE
% PERCENTUAL = PERCENTAGE OF SPECTRUM OVERLAY FOR ESTIMATE WELCH PERIODOGRAM

%MATERIAL
k = 5.988;
C = 3.216E21;

% SAMPLING TIME SETTING
PT_PERIODO = 2;

Fmin1 = 2;
Fmax1 = 4;
G1 = 2500
RMS_1 = sqrt(G1*(Fmax1-Fmin1));

Fmin2 = 20;
Fmax2 = 22;
G2 = 1000;
RMS_2 =sqrt(G2*(Fmax2-Fmin2));

%DEFINITION OF SPECTRUM CHARACTERISTICS
TAMANHO = 2^19;
PERCENTUAL = 99;

 F_INF = min(Fmin1, Fmin2);
F_SUP = max(Fmax1, Fmax2);
TAXA = F_SUP*2*PT_PERIODO;
FC = (F_SUP+F_INF)/2;
BANDA = (F_SUP-F_INF);
TAXA = F_SUP*2*PT_PERIODO;

SOBRE = round(TAMANHO*PERCENTUAL/100);

T = TAMANHO/TAXA;
TEMPO = T;

[t,Saa] = FILTRA_SINAL_2(T,RMS_1,RMS_2,Fmin1,Fmax1,Fmin2,Fmax2,TAXA,TAMANHO);


media = mean(Saa)
desv = std(Saa)
kurt = kurtosis(Saa)

pd_g = makedist('Normal','mu',media,'sigma',desv);

[c,hist,edges,rmm,idx] = rainflow(Saa/2);
```

```
[LINHAS, COLUNAS] = size(hist);

for i = 1:LINHAS
   NSa(i) = sum(hist(i,:));
   Sa(i) = (edges(i)+edges(i+1))/2;
   d(i,1) = (NSa(i)*Sa(i)^k)/C;
end
nsa = NSa;
NSa = NSa/sum(NSa);

figure(1)
plot(Sa,NSa);

figure(2)
plot(t,Saa);

figure(3)
h = histogram(Saa,20)
U = transpose(h.BinEdges);
[LINHAS, COLUNAS] = size(U);

for i = 1:LINHAS-1
   St(i) = (U(i)+U(i+1))/2;
   y(i) = pdf(pd_g,St(i));
end

DELTA_St = St(2)-St(1);
NSt = h.Values/(sum(h.Values)*DELTA_St);

plot(St,y,St,NSt)


V(:,1) = St;
V(:,2) = y;
V(:,3) = NSt;

G(:,1) = Sa;
G(:,2) = NSa/(G(2,1)-G(1,1));

figure(4)
bar(G(:,1),G(:,2))

 [pxx,w]= pwelch(Saa,2048,32,2048,'onesided',1/t(2));

figure(5);
bar(w,pxx);

P(:,1) = w;
P(:,2) = pxx;

Saaa = Saa(10000:30000);
Dac = sum(d)
D = Dac/TEMPO
Tf = 1/(24*3600*D)
```

Function [t,Saa] = FILTRA_SINAL_2(T,RMS_1,RMS_2,Fmin1,Fmax1,Fmin2,Fmax2,TAXA,TAMANHO);

```
function [t,Z] = FILTRA_SINAL(T,RMS_SINAL1,RMS_SINAL2,Fmin1,Fmax1,Fmin2,Fmax2,TAXA,TAMANHO)

% T = SIGNAL ACQUISITION WINDOW TIME
% RMS_SINAL = RMS VALUE OF THE SIGNAL TO BE GENERATED
% Fmin = LOWER LIMIT OF SIGNAL FREQUENCY BAND
% Fmax = UPPER LIMIT OF SIGNAL FREQUENCY BAND
%TAXA = SIGNAL ACQUISITION RATE
% TAMANHO = SPECTRUM SIZE
% PERCENTUAL = PERCENTAGE OF SPECTRUM OVERLAY FOR WELCH PERIODOGRAM ESTIMATE
```

```
t = linspace(0,T,TAMANHO);

R = rand(1);
rng(R);
X1 = randn(TAMANHO,1);
Y1 = bandpass(X1,[Fmin1 Fmax1],TAXA,'Steepness',0.9999,'StopbandAttenuation',10);

R = rand(1);
rng(R);
X2 = randn(TAMANHO,1);
Y2 = bandpass(X2,[Fmin2 Fmax2],TAXA,'Steepness',0.9999,'StopbandAttenuation',10);
 Z = RMS_SINAL2*Y2/std(Y2) + RMS_SINAL1*Y1/std(Y1);
```